



The Surface Proteome of Adult Neural Stem Cells in Zebrafish Unveils Long-Range Cell-Cell Connections and Age-Related Changes in Responsiveness to IGF

Jara Obermann,¹ Felicia Wagner,¹ Anita Kociaj,^{2,3,4} Alessandro Zambusi,^{2,4,5} Jovica Ninkovic,^{2,3,5} Stefanie M. Hauck,¹ and Prisca Chapouton^{6,*}

¹Research Unit Protein Science, Helmholtz Zentrum München, German Research Center for Environmental Health, Heidemannstrasse 1, 80939 Munich, Germany

²Institute of Stem Cell Research, Helmholtz Zentrum München, German Research Center for Environmental Health, Ingolstädter Landstrasse 1, 85764 Neuherberg, Germany

³Physiological Genomics, Biomedical Center, Ludwig Maximilian University Munich, Grosshaderner Strasse 9, 82152 Planegg-Martinsried, Germany

⁴Graduate School of Systemic Neurosciences, Ludwig Maximilian University Munich, Grosshaderner Strasse 2, 82152 Planegg-Martinsried, Germany

⁵Department of Cell Biology and Anatomy, BMC, Ludwig Maximilian University, Munich, Germany

⁶Research Unit Sensory Biology and Organogenesis, Helmholtz Zentrum München, German Research Center for Environmental Health, Ingolstädter Landstrasse 1, 85764 Neuherberg, Germany

*Correspondence: chapouton@helmholtz-muenchen.de

<https://doi.org/10.1016/j.stemcr.2018.12.005>

SUMMARY

In adult stem cell populations, recruitment into division is parsimonious and most cells maintain a quiescent state. How individual cells decide to enter the cell cycle and how they coordinate their activity remains an essential problem to be resolved. It is thus important to develop methods to elucidate the mechanisms of cell communication and recruitment into the cell cycle. We made use of the advantageous architecture of the adult zebrafish telencephalon to isolate the surface proteins of an intact neural stem cell (NSC) population. We identified the proteome of NSCs in young and old brains. The data revealed a group of proteins involved in filopodia, which we validated by a morphological analysis of single cells, showing apically located cellular extensions. We further identified an age-related decrease in insulin-like growth factor (IGF) receptors. Expressing IGF2b induced divisions in young brains but resulted in incomplete divisions in old brains, stressing the role of cell-intrinsic processes in stem cell behavior.

INTRODUCTION

In all organisms, developmental processes continue throughout life, overlapping with signs of aging. Many organs maintain stem cell niches after having reached maturation, in which mitotic activity allows for the generation of new differentiated cells. However, the frequency of mitotic activity slowly decreases. Levels of quiescence and cell-cycle entry change following mechanisms that are incompletely understood. This regulation of adult stem cells' quiescence or cell cycle, important both for the unwanted occurrence of cancers and for the desired repair of damaged tissues, remains a fundamental problem in biology.

In vertebrate brains, neural stem cells (NSCs) remain present in defined areas and give rise to new neuronal cells throughout life, albeit in a declining manner. In mammals, well-studied areas are the subependymal/subventricular zone (SVZ) lining the lateral ventricle, giving rise to neuronal cells populating the olfactory bulb as well as the prefrontal cortex in juvenile humans (Lim and Alvarez-Buylla, 2016), the subgranular zone (SGZ) of the hippocampal formation, generating new granule neurons in the dentate gyrus (Goncalves et al., 2016), as well as the hypothalamus (Recabal et al., 2017). The NSCs of

these areas display similar morphologies, being tanycytes in the hypothalamus, radial glia in the dentate gyrus of the hippocampus, and radial-shaped astrocytes in the SVZ (Chaker et al., 2016; Fuentealba et al., 2012; Maggi et al., 2014). A special feature of the SVZ is the mixture of radial astrocytes with ependymal cells (Mirzadeh et al., 2008), the latter being recruited only in case of injury (Carlen et al., 2009).

Several parameters influencing the recruitment into the cell cycle of NSCs have been defined: growth factors, cell-adhesion molecules and the extracellular matrix, contact with blood vessels, cerebrospinal fluid, and metabolism (Goncalves et al., 2016; Lim and Alvarez-Buylla, 2016; Rafalski and Brunet, 2011). As aging progresses, the fraction of mitotically active NSCs declines (Capilla-Gonzalez et al., 2014; Kuhn et al., 1996). Several mechanisms of cell-intrinsic and cell-extrinsic nature, leading to this overall reduction of activity of NSCs, have been revealed. Stem cells have been shown to divide only a limited number of times in the dentate gyrus (Encinas et al., 2011) and reveal signs of depletion in the SVZ too (Calzolari et al., 2015). Progressive lengthening of the G₁ phase of NSCs might be a factor for their less frequent recruitment (Daynac et al., 2014, 2016). The milieu has also been shown to play a role in parabiosis experiments, exchanging the





lymphatic system of young and old mice (Villeda et al., 2011). The levels of distinct growth factors progressively change with age: insulin-like growth factor 1 (IGF1), fibroblast growth factor (FGF), and vascular endothelial growth factor decline in the dentate gyrus (Kang and Hebert, 2015; Shetty et al., 2005). The immediate surrounding niche, made of the neighboring cells and the extracellular matrix, known to play a role in stem cell activity (Kazanis et al., 2010; Porlan et al., 2014), might also be subjected to age-related changes influencing mitotic activity (Yamada et al., 2017). A clear picture to explain the individual behaviors within stem cell populations is nevertheless missing.

In the adult zebrafish brain, transcription factors homologous to their mammalian counterparts are at play in the neurogenic process (Diotel et al., 2015), making it a valid comparative vertebrate model organism. Moreover, it presents the advantage of a broader neurogenic activity within all brain regions and a high regenerative potential (Alunni and Bally-Cuif, 2016; Baumgart et al., 2012; Grandel and Brand, 2013). The radial glia in zebrafish display similar features to those of the NSCs of the mammalian neurogenic areas. Their somata are in immediate contact with the ventricles, they express the intermediate filaments glial fibrillary acidic protein (GFAP), Nestin, and Vimentin, and generate new neurons and glial cells (Kroehne et al., 2011; Rothenaigner et al., 2011). Their transitions back and forth between quiescence and cell cycle have been shown by long-term bromodeoxyuridine tracing and by Notch blocking experiments (Chapouton et al., 2010; März et al., 2010). Whether every cell or only a subpopulation enter the cell cycle regularly remains uncertain (Dray et al., 2015). The radial glia might give rise to newly born neurons through a direct conversion process without an immediately preceding mitosis (Barbosa et al., 2015). Additionally, progenitors without GFAP expression are also present in close proximity to the somata of the radial glia and are considered intermediate progenitors, even if similar cells organized in pools function as stem cells in other regions of the brain (Galant et al., 2016; Kaslin et al., 2009, 2017; Than-Trong and Bally-Cuif, 2015).

In addition to the abundance of NSCs, a major advantage of the zebrafish brain is the architecture of its pallium (dorsal telencephalon), where the ventricular surface opens on the outside instead of enclosing a lumen, due to an eversion process during embryonic development (Wullmann and Mueller, 2004), thus becoming accessible to imaging or manipulations (Barbosa et al., 2015; Dray et al., 2015).

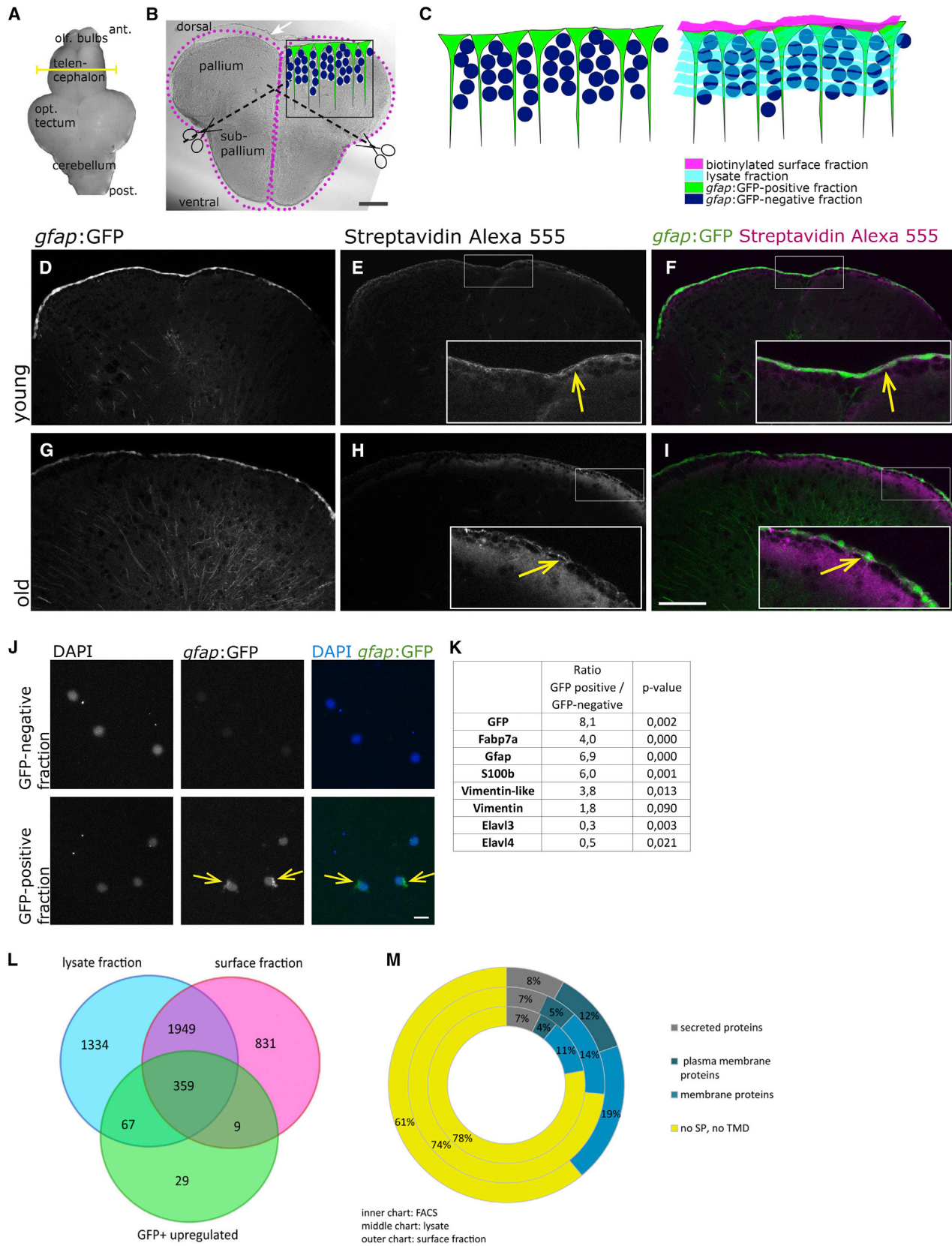
We made use of this architecture to isolate the proteins present in an intact population of NSCs. As this cell population reveals an age-related increase of quiescent cells (Edelmann et al., 2013), we identified the surface prote-

ome of the young and old ventricular zone to obtain sets of proteins likely implicated in the intercellular communication and in the regulation of cell cycle and quiescence. We focused on two aspects of the dataset. The significant over-representation of filopodial and lamellipodial protein components allowed us to discern new morphological features of NSCs. Furthermore, age-related changes revealed a decline in IGF1-receptor (IGF1R) expression, observed by both mass spectrometry and immunocytochemistry of the phosphorylated IGF receptor. This decrease was measurable by an altered response to the ligand IGF2b, able to induce complete cell divisions in young, but not in aged animals.

RESULTS

Identifying the Proteome of Neural Stem Cell Surfaces in Intact Brains

The closest contacts between the radial glia are at the level of their cell bodies, adjacent to the brain ventricle. With the aim of defining signaling pathways putatively implicated in their intercellular communication, we designed an approach to isolate all proteins present on the cell bodies in a native configuration of freshly isolated brains. The biotinylation protocol allowed the binding of biotin to the proteins expressed on the surface of the radial glia (Figures 1A–1C). We tested two different protocols of biotinylation, based on either covalent coupling to glycosyl side chains or covalent coupling to free amino groups of the proteins. We observed a systematic bias toward increased expression levels in old brains with the glycosylation-dependent biotinylation (Figure S1A), which might indicate age-dependent altered total glycosylation levels. While the majority of proteins identified by the glycosylation-dependent biotinylation was also identified by the direct amino acid binding biotinylation (Figure S1B), we obtained a higher number of proteins with the latter protocol, and concentrated our further analysis on those results. Three replicates of 6–7 brains (2-year-old and 4-month-old, respectively) were prepared in parallel. To verify the localization of biotin anchoring, we fixed two brains and incubated them with streptavidin-AlexaFluor 555. Both young and old brains revealed a specific surface anchorage of biotin with a minor penetration below the row of radial glia (Figures 1D–1I), indicating the validity of the method. After biotinylation, brains were dissected into pallium and subpallium (Figure 1B) in order to separate the apical part of the radial glia located on the dorsal surface, where we expect cell-to-cell communication to take place, from their basal endfeet located on the ventral pial surface. After tissue lysis, biotinylated proteins were bound to streptavidin beads, proteolyzed, and analyzed by mass spectrometry.



(legend on next page)



The non-biotinylated proteins, representing the remaining material of the telencephalon (Figure 1C, lysate fraction) were also analyzed by mass spectrometry. We compared the results obtained by this approach, with proteins from sorted radial glia of the telencephalon of *gfap*:GFP transgenic fish (fluorescence-activated cell sorting [FACS] scatterplots in are shown in Figures S2A–S2F and 1J). These experiments revealed consistent clustering of the GFP-positive and GFP-negative fractions by principal component analysis (Figure S2G), and an even distribution of proteins respectively up- and downregulated (Figure S2H). The set of proteins enriched in the GFP-positive fraction contained expected proteins known to be expressed by radial glia (GFP, GFAP, S100 β , FABP7a/BLBP, Vimentin) (Ganz et al., 2010; März et al., 2010) while the GFP-negative fraction was enriched in proteins present on differentiated neurons (Elavl3/HuC, Elavl4/HuD) (Adolf et al., 2006; Grandel et al., 2006) (Figure 1K). A high number of proteins in the biotinylated fraction was not present in the FACS-GFP-positive cells, which might be due to a loss of proteins during the enzymatic dissociation of the cells. Conversely, a large proportion (79.3%) of the proteins isolated from the FACS-GFP-positive cells were also identified in the biotinylated fraction (Figure 1L). According to our experimental design, this overlap is expected to be incomplete, as FACS-sorted cells contain in addition to plasma membrane the whole cytosolic fraction of radial glia (Figure 1C). GeneRanker analysis of the FACS-GFP-positive fraction revealed overrepresentation of the insulin pathway, cannabinoid receptor 1 pathway, glial cell line-derived neurotrophic factor (GDNF) and platelet-derived growth factor receptor β (PDGFR β) signaling pathways (Table S1A). While sorting cells by FACS allows for the analysis of the whole content

of proteins in a certain cellular type, the advantage of the biotinylation approach was to isolate proteins of intact, non-dissociated cells.

Phobius analysis was used to assess the proportion of proteins with transmembrane domains and signal peptides (Figure 1M). The surface biotinylation technique led to a protein set enriched in membrane proteins compared with the lysate fraction and the FACS-sorted cells fraction. Of the proteins listed in the Genomatix Pathway System, 645 belong to the plasma membrane, 51 are localized in the cell cortex, 145 are cytoskeletal binding proteins, and 43 are cell-adhesion molecule binding proteins.

Taken together, comparison of the datasets obtained from sorted radial glia, biotinylated surface fraction, and the non-biotinylated lysate of the telencephalon (for original dataset files see Table S6) indicate that the biotinylation approach specifically isolates proteins expressed on the surface of the stem cell compartment.

Identified Proteins Indicate an Epithelial Character and Display a Group Associated with Lamellipodia and Filopodia

The radial glia, as opposed to embryonic neuroepithelial cells, do not form a columnar epithelium, but their somata are cone-shaped and are connected laterally to each other only by a thin apical junctional region. Their highly branched radial processes extend far into the parenchyme. Considering this morphology, it is interesting to define to which extent these cells reveal an epithelial character. In the list of identified surface proteins, members with specific apicobasal localizations appeared (Table 1). For instance, proteins involved in formation of tight junctions (i.e., Discs large 1 and 3, Junctional Adhesion Molecule 3,

Figure 1. Proteome Identification

- (A) The biotinylation reaction was performed on freshly isolated brains. The yellow line depicts the location of the cross-section shown in (B).
- (B) Cross-section through the telencephalon of a zebrafish. Biotinylated surfaces are depicted as magenta dots. The upper surface of the pallium borders the ventricle, located below the tela choroidea (white arrow) and is composed of the cell somata of the radial glia (depicted in green in the inset). The midline between both hemispheres is also filled by a thin part of the ventricle. After the biotinylation reaction, telencephalons were separated into the dorsal part (pallium) and ventral part (subpallium).
- (C) Drawing of the fractions isolated by FACS and by biotinylation, depicting in green the radial glia, in dark blue the remaining cells of the telencephalon, in magenta the biotinylated fraction containing the cell surfaces of the radial glia, and in light blue the lysate fraction containing the remainder of these cells as well as the rest of the telencephalon.
- (D–I) Histochemistry on cross-sections with streptavidin coupled to AlexaFluor 555 after biotinylation of the brain, revealing the expected binding of biotin on the cell surfaces in young (D–F) and old (G–I) brains.
- (J) Cells of the GFP-positive and -negative fraction plated directly after the sorting; nuclei are stained by DAPI.
- (K) Known proteins isolated on FACS-sorted radial glia.
- (L) The overlaps between the surface fraction, lysate fraction, and GFP-positive fraction are represented. The majority (79.3%) of proteins identified in the FACS-GFP-positive fraction were also found in the biotinylated fraction.
- (M) Identified proteins were categorized according to the presence of signal peptides and transmembrane domains, revealing an enrichment of plasma membrane proteins in the biotinylated fraction compared with the lysate and to the FACS-retrieved proteins.
- Scale bars, 100 μ m (B and I) and 10 μ m (J).



Table 1. Biotinylated Fraction: Proteins Indicating the Epithelial Character of the Radial Glia and Proteins Associated with Filopodia and Lamellipodia

Cell-Cell Adherens Junctions p value: 1.23×10^{-3} No. of genes (observed): 13 No. of genes (expected): 5.09 No. of genes (total): 54	CDH2, ACTN1, DSP, FLOT1, CTNNB1, DAG1, CADM4, NDRG1, FLOT2, CTNNA1, GJA1, CADM1, CTNNA2
Bicellular tight junctions p value: 7.60×10^{-3} No. of genes (observed): 19 No. of genes (expected): 10.5 No. of genes (total): 111	ANK3, DLG3, RAP2B, CTNNB1, CXADR, MAGI1, TBCD, AOC1, STRN, FZD5, MTDH, ADCYAP1R1, RAP2C, VAPA, RAPGEF2, LIN7A, JAM3, DLG1, LIN7C
Gap junctions	CX43; +FACS dataset: Cx28.8
Apical plasma membrane p value: 8.38×10^{-3} No. of genes (observed): 40 No. of genes (expected): 27.2 No. of genes (total): 288	AP2A1, CDH2, FLOT1, CD81, ANO1, CLCN3, BMPR2, TF, ATP2B1, PRKAA1, FLOT2, SHANK2, ATP1B1, MTDH, ATP6V1E1, PDGFRB, ATP6VOD1, CNTFR, TMEM30A, GJA1, GNAT3, RAB14, CD36, STXB3, ATP6V1A, RAB27B, RAPGEF2, NOD1, KCNA1, SORBS2, PTPRO, PTEN, ATP8B1, CSPG4, FZD3, PTK2, KCNN4, SEPT7, ITPK1, SLC7A5
Basolateral plasma membrane p value: 5.27×10^{-6} No. of genes (observed): 41 No. of genes (expected): 19.8 No. of genes (total): 210	ENPP1, SLC4A4, AP2A1, CDH2, ANK3, DLG3, DSP, FLOT1, SLC12A6, SLC38A3, CTNNB1, CXADR, NDRG4, DAG1, BMPR2, TF, ATP2B1, FLOT2, ATP1B1, CNM2, PALM, CADM1, ARRB1, STXB3, ERBB4, ANK1, NOD1, MPZ, LIN7A, CTNNA2, HEPH, DLG2, ARRB2, SLC1A3, DLG4, ANXA2, CASK, DLG1, KCNN4, LIN7C, EGFR
Filopodium formation (integrin signaling) p value: 2.01×10^{-2} No. of genes (observed): 27 No. of genes (expected): 18.3 No. of genes (total): 123	BCAN, SMC3, ITGAV, GPC1, LAMB3, GPC4, RAP1B, COL4A1, COL1A1, BRAF, CDC42, TLN1, MAPK1, DOCK3, ITGB5, AGRN, SHC3, TLN2, ITGB7, ITGB2, KRAS, MAP2K1, DOCK10, ITGB4, COL15A1, PTK2, GRB2 Y-branching of filopodia: ACTR2, NCKAP1, CDC42, ARPC3, ARPC2, PSMA7, RAC1
Lamellipodium p value: 1.74×10^{-7} No. of genes (observed): 39 No. of genes (expected): 16.2 No. of genes (total): 172	MYH10, RAC2, RUFY3, CDH2, FLOT1, ITGAV, CTNNB1, NCKAP1, SLC39A6, PPP1R9A, DAG1, FERMT2, FGD1, FLOT2, CTTN, ARPC3, GSN, CTNNA1, FSCN1, PPP1R9B, CDK5, APP, DPYSL3, SORBS2, CTNNA2, BRK1, CORO1A, ENAH, NRBP1, PTPRO, DBNL, CSPG4, PTK2, ITSN1, CARMIL2, SRCIN1, ABI2, DGKZ, PTPRZ1

Metadherin, Striatin, Ankyrin3) and in cell-cell adherens junctions (i.e., Dystroglycan 1, N-Cadherin, Catenin- β 1, - α 1, and - α 2, Desmoplakin) were identified (Table 1). Therefore, even if this adult ventricular surface on the dorsal pallium is classically not considered as a neuroepithelium, these cells that pave the whole ventricular surface express epithelial marker proteins.

We observed a group of proteins involved in filopodia and lamellipodia formation (Table 1), such as CDC42, RAC1 and -2, DOCK 3 and 10, Integrin α 5 β 2 and β 7, RUFY3, BRK1, Formin-like 3, and Fascin 1a and 1b. The high ramification of radial glia in the parenchyme (inset in Figure 2C) might explain this finding. However, as the biotinylation was specifically targeting the apical surface and could not reach the deep processes, we wondered whether filopodia are present apically. Indeed, different expression levels occurred predominantly between the ventral and dorsal domains of the telencephalon (Figure 2A). We performed morphological analyses of single cells by lipofections *in vivo*, using either a combination of two plasmids (EF1 α : Gal4 and UAS: mtdTomato) or a single plasmid (pCS2-Lifeact-RFP) highlighting F-actin, to label the membrane of a few scattered cells. The infusion of the lipofection mix into the brain ventricle led in all cases to an exclusive expression in the radial glia (Figures 2B–2D, yellow arrows). We took serial confocal pictures to obtain z stacks of whole-mount brains with mtdTomato membrane staining. Lamellipodia were observed in some cells that overlapped with the apical surface of a neighboring cell (Figures 2E–2G). In the majority of analyzed cells, we identified at least one filopodium-like extension. The extension was either extending apically along borders between two cells (Figures 2H–2J), reaching the second next cell, or extending from the basolateral cell surface and reaching apical locations of neighboring cells, furthest to the fourth *gfap*:GFP-positive cell (Figures 2K–2P). We used a Lifeact construct and analyzed 23 cells from 3 sectioned brains. The cellular extensions contained Lifeact labeling, revealing the presence of F-actin (Figures 2Q–2S). Co-lipofections of Lyn-GFP and Lifeact-RFP plasmids showed that the cellular extensions could be distinct in their composition, as a few of them were not labeled by Lifeact (Figures 2T–2V').

Since the mass spectrometric analysis showed some differences with age in the expression levels of some filopodia-associated proteins, such as the downregulated Neuroigin 1 and FARP1, and the upregulated Flotillin 2, Gelsolin, Talin 2, and Src kinase signaling inhibitor 1 (Figure 2A), we compared morphologies and performed measurements of length and number of filopodia on 16 young (3-month-old) and 26 old (2-year-old) mtdTomato-labeled cells (Figure S3). Neither the mean size of these extensions, nor their numbers, varied significantly between young and old

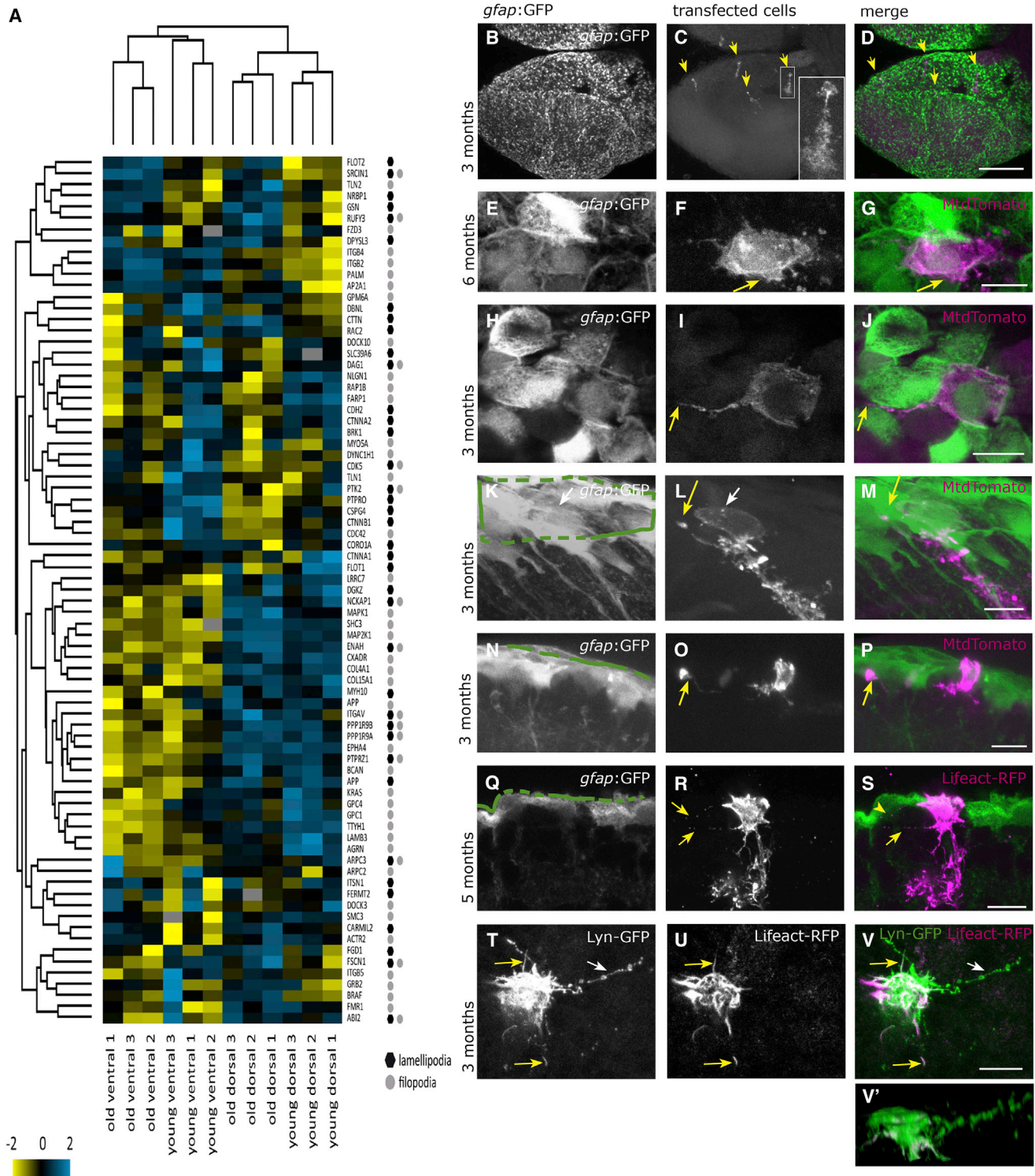


Figure 2. Proteins Associated with Lamellipodia and Filopodia, Detected in Apical and Basolateral Locations of the Radial Glia
 (A) Hierarchical clustering for proteins associated with lamellipodia and filopodia, revealing that some of them display age-related changes.
 (B–V') Lipofections *in vivo* were performed and imaged after fixation as whole-mount preparations or as sections (Q–S). (B–D) Overview of one telencephalic hemisphere visualized from the top onto the dorsal surface as a maximum-intensity projection. (B) Cell bodies of the
 (legend continued on next page)



brains (Figures S3J–S3K). Nevertheless, possible structural alterations might exist and will need to be examined in future studies.

Together, these results reveal cellular extensions between the cell bodies of NSCs, which might promote cell-to-cell communication ranging up to 4 cells apart.

Signaling Pathways Active in the Surface Fraction

Besides a possible communication via filopodial extensions, other candidates might relay intercellular signals, such as the gap-junction protein Cx 43, or Cx 28.8 identified in the GFP-positive FACS fraction. We further identified a high number of proteins (557) associated with extracellular exosomes that might convey signals.

We examined pathways significantly overrepresented on the dorsal versus ventral side of the telencephalon, hence likely involved in the communication at the apical location of the radial glia. GeneRanker analysis revealed among others the planar cell polarity, brain-derived growth factor, Semaphorin, and Eph receptor pathways (Table S2).

Cell-surface receptors and their differential expression are listed in Figure S4A. We identified, for instance, Notch3 as well as Dner, another Notch family member, and receptors for GDNF, ciliary neurotrophic factor (CNTF), PDGF, epidermal growth factor (EGF), bone morphogenetic protein (BMP), FGF, and WNT. Many of these receptors and ligands were missing in the proteins identified from cells isolated by FACS, possibly due the enzymatic dissociation. We nonetheless confirmed the expression of these signaling molecules in the radial glia by RNA sequencing (RNA-seq) analysis of FACS-sorted GFP-positive and -negative fractions (Figure S4B).

Following the intriguing finding of filopodia on the radial glia, we tested whether they would relay signals identified here in the biotinylated fraction, similarly to results obtained in other cells with filopodia (Prols et al., 2016). We investigated the co-localization of two signaling pathways in the cellular protrusions, Wnt and EGF.

The localization of Wnt signals was examined (Stanganello et al., 2015) in NSCs co-lipofected with Wnt8a-

mcherry and Lyn-GFP. Lipofected cells did reveal a dotted localization of Wnt8a-mCherry (Figures S5B, S5E, S5H, and S5K), also at the edges of the cell soma close to neighboring cells. However, no clear co-localization with filopodial extensions could be identified (Figures S5A–S5I). In a second approach, we expressed a GFP-tagged secreted Wnt receptor SFRP1a-GFP in HEK-293 cells and collected the supernatant, then applied it on fixed floating brain sections. As a positive control, lipofected cells with Wnt8a-mCherry did not show a strong specific co-localization of SFRP1a-GFP (Figures S5J–S5L). Cells lipofected with Fyn-RFP to visualize the filopodia did not reveal co-localization of the SFRP1a-GFP (Figures S5J–S5L). We therefore conclude that with the methods used here, filopodial extensions in adult NSCs do not seem to convey Wnt signaling.

The localization of the EGF receptors was probed with an AlexaFluor 488-EGF complex that binds EGF receptor (EGFR) (Pastrana et al., 2009). Sections with cells lipofected with mtdTomato were incubated with the green fluorescent complex, revealing the localization of EGFR on the radial glia (Figures S5P–S5W). The AlexaFluor 488-EGF complex did not co-localize specifically with filopodial extensions. Hence, potential signals relayed via filopodia to neighboring radial glia remain to be determined in further studies.

As we were looking for signals involved in the regulation of recruitment to the cell cycle, we next focused on pathways differentially regulated in young and old brains.

The IGF Signaling Pathway Diminishes with Age, and the Mitotic Response to IGF2b Becomes Incomplete

The differential protein content in young and old surface fractions revealed an enrichment in proteins involved in G₁/S transition in the young brain, and an enrichment in proteins involved in the P21 (CDKN1A) pathway in the old brain (Tables S3 and S4), in accordance with previously observed age-related decrease in mitotic activity (Edelmann et al., 2013). Hierarchical clustering and principal component analysis revealed consistent results between replicates (Figures 3A and 3B). The proteins up- and

radial glia are labeled by the gfap:GFP transgene. (C) A small, variable number of cells per brain were labeled by the *in vivo* lipofection (maximum 12 cells per brain); their somata and branched radial processes into the parenchyme are visible (inset is a higher magnification), revealing the soma at the top (apical side) and the radial process in the parenchyme with numerous branches. All lipofected cells displayed this radial process, but it is not visible on all pictures. (D) Merged channels. (E–G) Apical surface of one radial glia, viewed from the top, depicting the existence of lamellipodia extending laterally (arrow in F and G). (H–J) Apical surface of one radial glia, depicting the existence of filopodia (arrow in I and J). (K–M) Filopodia are also extending from the basolateral cell surface toward apical locations on neighboring cells (arrow in L and M). (N–P) The longest filopodia span below 4 cell diameters. (Q–S) lipofection with Lifeact-RFP also reveals basolateral extensions (arrows in R and S). (T–V) Apical view on a cell co-lipofected with the membrane-localized Lyn-GFP (T) and the F-actin localized Lifeact-RFP (U) revealing the presence of filopodial extensions with F-actin (yellow arrows) or without (white arrow). (V') Lateral view of the same cell. Green lines in (K), (N), and (Q) depict the ventricular surface. Scale bars, 100 μ m (D) and 10 μ m (G, J, M, P, S, and V).

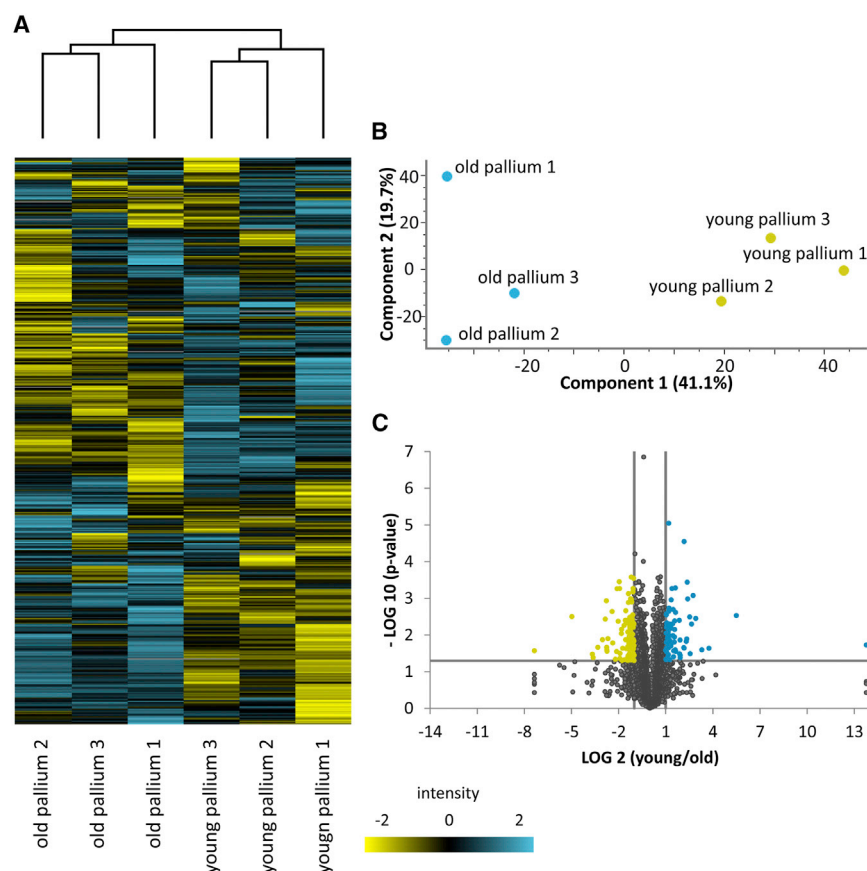


Figure 3. Expression Changes with Age in the Ventricular Zone

(A) Hierarchical clustering of all proteins in the ventricular zone using normalized log₂ transformed abundances of three old and three young brain samples (high-abundance proteins colored blue, low-abundance proteins yellow).

(B) Principal component analysis of the three samples of old brain and three samples of young brain.

(C) Volcano plot analysis: ratios of the means of all protein abundances in the three old compared with the three young brain samples were plotted against the corresponding negative log₁₀ transformed p value.

downregulated with age were evenly distributed (Figure 3C). Several components of N-Cadherin signaling were upregulated in young surfaces (N-Cadherin signaling components, p value 6.14×10^{-3} ; DAGLA, CDH2, CDC42, CTNNA1, KIF5B), suggesting that cell-cell interactions might be modified with age. However, other components of this signaling pathway remained unchanged (CTNNA1, CNR1, GRIA2, CTTN, GSN, GJA1).

Proteins on the NSCs' surface and in the lysate revealed a decrease in IGF signaling with age (Figures 4A and 4B), especially for the receptors IGF1R and insulin receptors. In zebrafish, two *igf1r* genes, *igf1ra* and *igf1rb*, are orthologous to the mammalian Igf1R and play complementary roles during development (Schlueter et al., 2006). Both were decreased on the surface fraction of aged brains. The insulin receptor InsR-B also declined with age, while the level of InsR-A expression did not change. IGF ligands were not detected in the proteomic analysis, but were detected by RNA *in situ* hybridization (Figure S6), suggesting that they might act as autocrine or paracrine factors, as in mammalian adult neurogenic areas (Bracko et al., 2012; Lehtinen et al., 2011). Phosphorylated (phospho-)IGF1R expression was visible in immunostainings in the layer of radial glia, as well as in a few closely located cells in the pa-

renchyme in young brains (Figures 4C–4F and 5A–5D), while in aged brains only a few plasma membrane-localized dots and a weak cytoplasmic expression were visible in the radial glia (Figures 4G–4J and 5I–5L).

IGF2b was cloned into a 5× UAS plasmid for overexpression by *in vivo* lipofections. Fish were lipofected with a red-labeling plasmid alone or in combination with *igf2b*. Control

lipofections with two differently colored plasmids resulted in cells receiving both plasmids in 90% of the cases (27 of 30 cells co-lipofected with plasmids for a green cytoplasmic staining and for a membrane-bound red staining revealed expression of both colors). After 2–4 days, we observed an increased expression of phospho-IGF1R in the cells lipofected with *igf2b* (Figures 5E–5H, arrows in 5G and 5H) as well as in their neighbors, indicating the expected effect of IGF2b expression. The phospho-IGF1R expression in aged brains, upon either control lipofections (Figures 5I–5L) or *igf2b* lipofections (Figures 5M–5P), showed a lower basal expression than in young brains, and IGF2b overexpression was able to induce a few dots of phospho-IGF1R expression (arrows in Figures 5O and 5P). However, the expression was not as strongly increased as in young brains, in line with the decreased receptor expression with age observed by mass spectrometry. Quantification of the fluorescence confirmed higher expression levels in *igf2b*-lipofected cells compared with control lipofections in young brains, but no significantly detectable change in old brains (Figure 5Q). We tested another downstream target of IGF2b signaling, phosphorylated Akt (Ser473), which revealed only very low levels of expression (Figure S7).

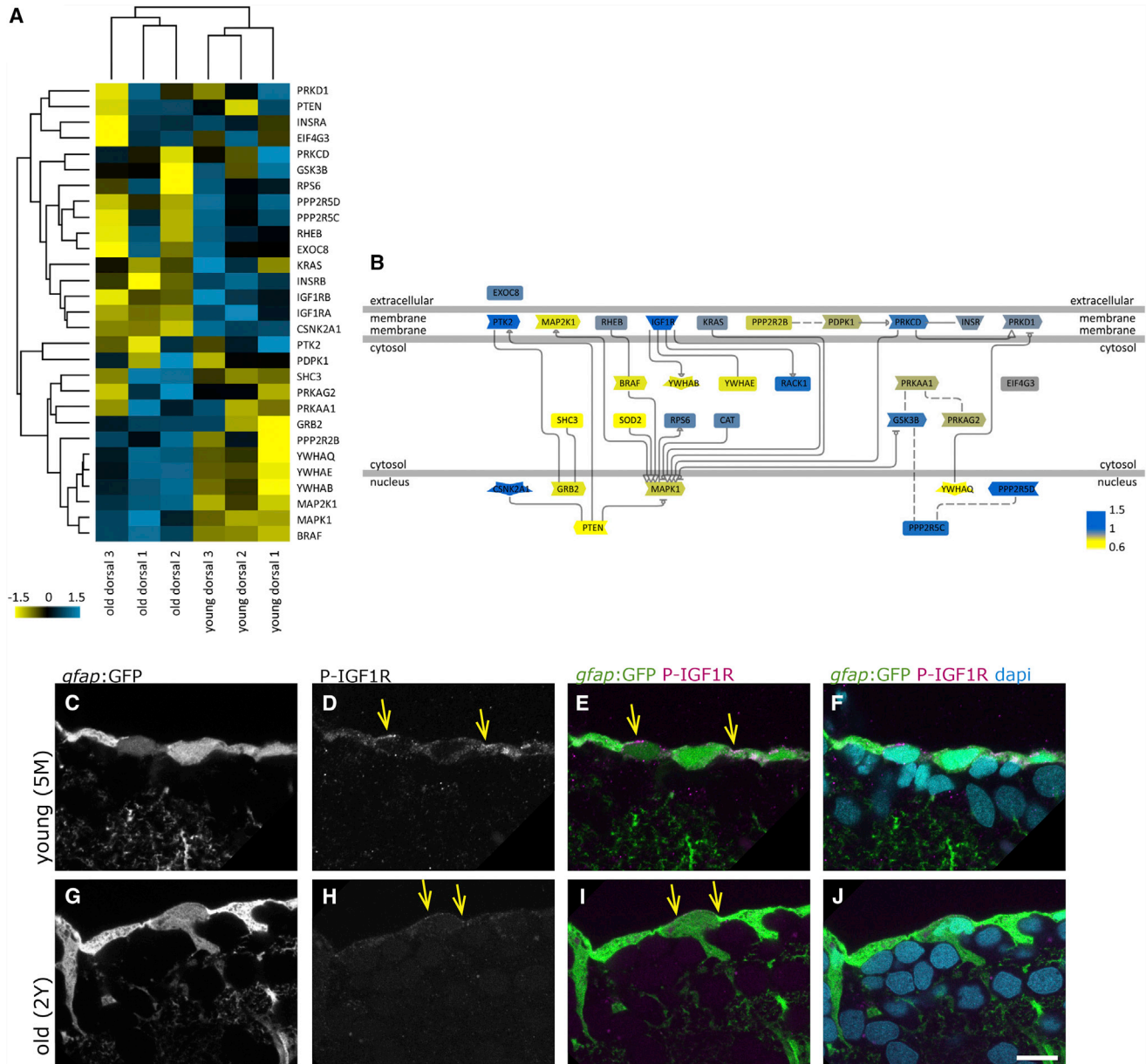


Figure 4. The IGF Signaling Pathway Declines with Age

(A) Hierarchical clustering of the IGF, Insulin, and Akt pathway protein members identified in the surface fraction, revealing the differential expressions in young and old dorsal surface fractions (scale: \log_2 young/old). Insulin receptor B, as well as IGF1 receptors a and b, are downregulated with age, while some other components are upregulated (i.e., MAP2K1 and BRAF).

(B) Representation of the signaling pathway with color coding (blue, upregulated young; yellow, upregulated old).

(C–J) Phosphorylated IGF1R (P-IGF1R) immunohistochemistry (Tyr1161) on young (5 months, C–F) and old (2 years, G–J) brains as a close-up view on the ventricular surface of the dorsal pallium depicted as single confocal planes. The radial glia somata, located at the border of the ventricle, express P-IGF1R (yellow arrows). We observe the distinct expression levels of P-IGF1R in young and old brains in a total of 4 young and 4 old immunosamples. Scale bar, 10 μ m.

To test for functional downstream effects of IGF in the adult NSCs, we analyzed the putative proliferative effect 2–5 days after lipofection in 6 independent experiments. Overexpression of IGF2b in young brains (2–4 months

old) resulted in a higher proportion of lipofected cells that revealed a recent mitosis, being visible as two neighboring cells immediately abutting each other (Figures 6A–6H and 6X; Table S5). Even if the cell division response to

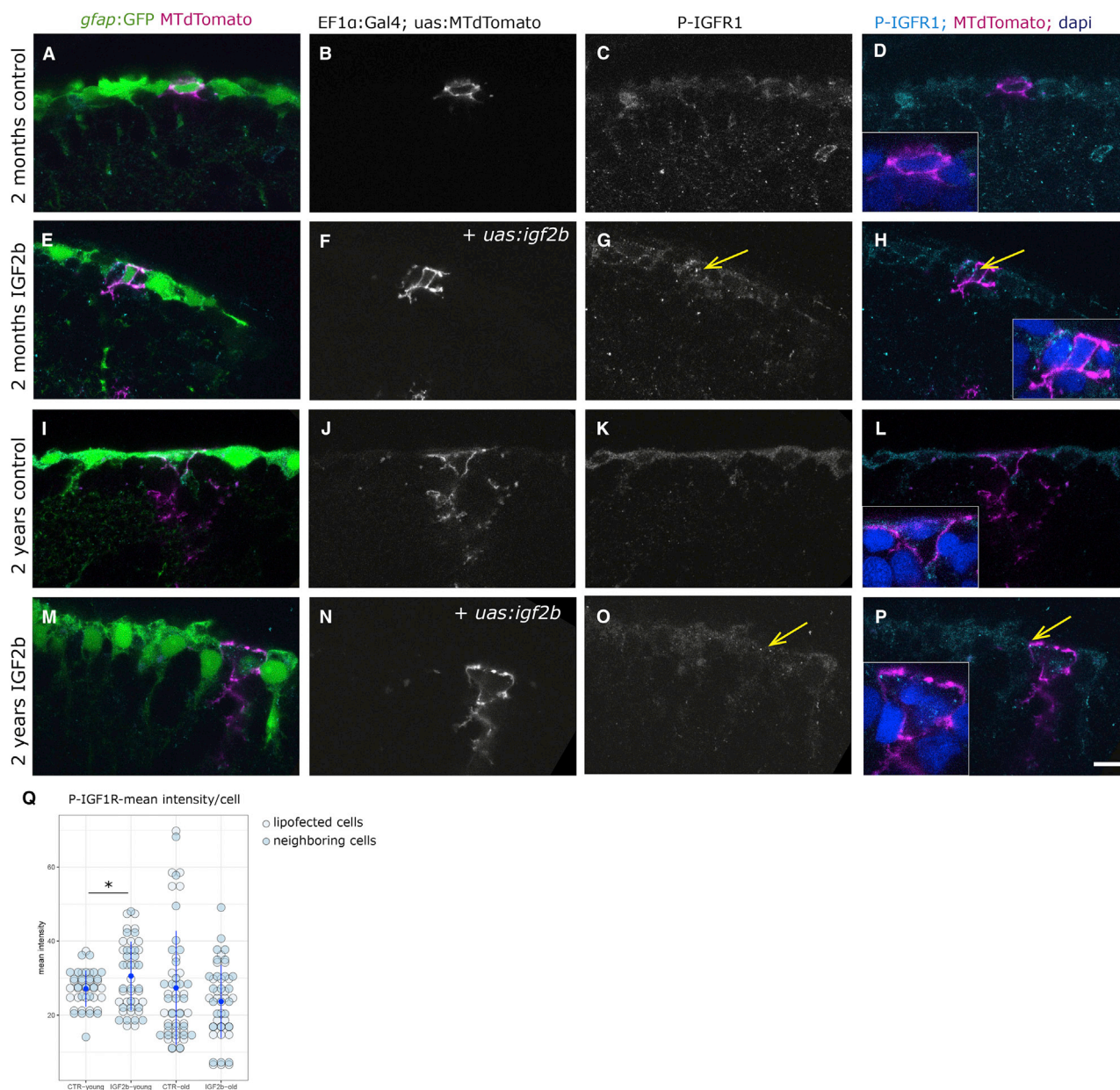
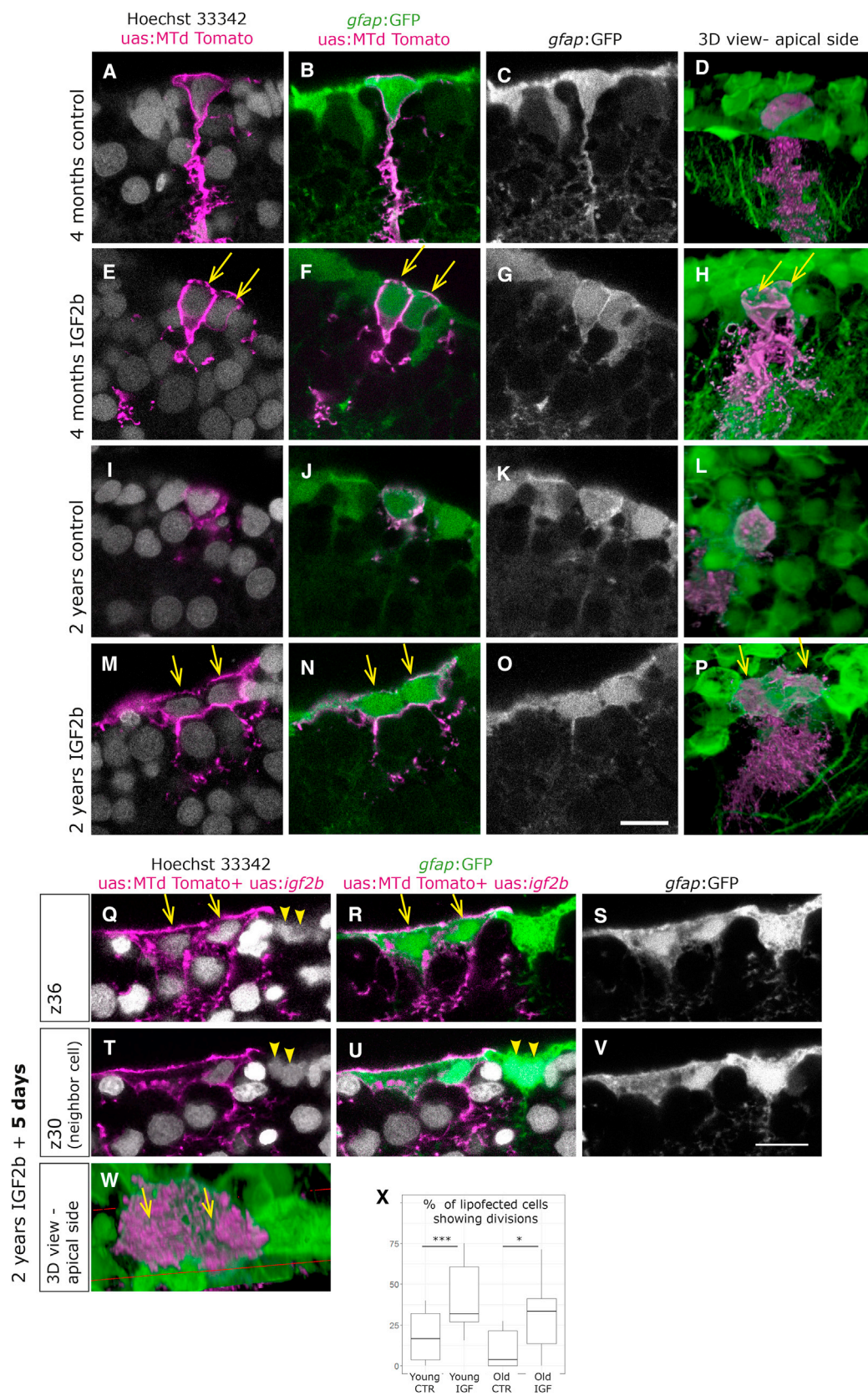


Figure 5. IGF2b Overexpression Activates the IGF1R in Lipofected Cells

(A–P) P-IGF1R immunohistochemistry on young (A–H) and old (I–P) brains. The radial glia are labeled by the *gfap:GFP* transgene. Single cells in magenta have been lipofected *in vivo* 4 days prior to brain fixation with mtdTomato (control, A–D and I–L) or with mtdTomato and *igf2b* (IGF2b, E–H and M–P), highlighting primarily the cell soma (the radial process is not always in the plane of the optical section, but it is present below the somata of lipofected cells). We observe the distinct expression levels of P-IGF1R in young control (C and D), young + IGF2b (highest, arrows in G and H), old control (K and L), and old + IGF2b (a few dots, arrows in O and P). Insets in (D), (H), (L), and (P) are close-ups of the lipofected cells; nuclei in blue stained by DAPI. Single confocal planes are displayed. Scale bar, 10 μ m.

(Q) The mean intensity of the phospho-IGF staining was measured on 7 lipofected cells and their immediate neighbors in each condition. Staining intensities differ significantly between control and *igf2b*-lipofected brains (t test; $p = 0.030$) in young but not in old brains.



(legend on next page)



IGF2b was indeed observed in a higher proportion than in control cells, it did not occur in all transfected cells, suggesting that the cells do not all have the same capacity to respond. Note that in [Figures 5E–5H](#), the lipofected cell has divided and encompasses two cell bodies, even if the two cells are incompletely covered by the membrane staining. Overexpression of IGF2b in old brains was able to also induce the formation of two nuclei; however the division was incomplete, lacking cytokinesis, and led to the formation of very large cells ([Figures 6I–6P](#) and [6X](#)). More time might be required for old cells to undergo cytokinesis, so we extended the lapse to 5 days, which revealed, however, the same effect of binucleation in old cells ([Figures 6Q–6S](#) and [6W](#)). We also observed that some cells next to the *igf2b*-lipofected cells revealed the same phenotype of binucleated cells, as they might respond in a paracrine manner to IGF ([Figures 6T–6V](#)). The incomplete divisions might be the result of the lowered levels of IGF receptor, and the exact downstream mechanism will require closer examination. Together, our results show that aged cells are not competent to respond and divide properly to an increase of growth signals encountered, hence indicating significant cell-intrinsic alteration in the course of aging.

DISCUSSION

With the aim of understanding better how NSCs communicate and organize their cell-cycle entries, we identified the proteins expressed on their surface in young and aged brains. The use of the zebrafish brain, offering direct access to NSCs without preceding dissociation, combined with a biotinylation method, permitted us to obtain the surface proteome of an intact NSC population. From there we showed the presence of apically located filopodial structures and a changing response to IGF with age. Hence, two important aspects are revealed herein: a possible path of intercellular communication via cellular extensions, and cell-intrinsic alterations impacting on the proliferative competence of aging cells.

One of the two biotinylation protocols employed in this study, involving a covalent binding reaction between glycosylated residues and biotin, revealed a strong bias for proteins increased in aged samples, suggesting increased glycosylation patterns with aging. Age-related changes in glycosylation patterns in the brain have previously been reported ([Miura and Endo, 2016](#)), and a closer investigation of these alterations will be important.

The identified proteins in the surface fraction were in accordance with previous findings in the zebrafish or other adult neurogenic systems. For instance, Connexin 43, identified here on the adult radial glia in zebrafish, plays a role in the adult neuroepithelium in mammals ([Lacar et al., 2011](#)). The representation of exosome components in our study is interesting in the context of their newly described roles in adult neurogenesis ([Batiz et al., 2015](#)). We also identified Notch3 and Dner, in keeping with the role for the Notch signaling pathway described in previous studies ([Alunni et al., 2013](#); [Chapouton et al., 2010](#); [Ehm et al., 2010](#); [Hsieh et al., 2013](#); [Katz et al., 2016](#)).

Our study reveals protein members that allow defining an epithelial identity of the adult NSCs, a question that was also addressed by [Grupp et al. \(2010\)](#), who observed the presence of ZO-1 in those cells. A new feature of the cells described here is the presence of lateral lamellipodial and filopodial extension from the somata of the radial glia. The filopodial extensions are contacting neighboring cells further than the next neighbor (up to the fourth, most frequently the second), an aspect that might be important for cell-to-cell communication over several cell distances. Filopodia can convey signals in developing tissues ([Prols et al., 2016](#)), such as Wnt signals ([Stanganello et al., 2015](#)) or Notch signals ([Cohen et al., 2010](#)). Such signals remain to be identified in these adult cells, and could possibly be involved in coordinating the cell-cycle activity. A feedback signaling between cycling cells and their neighbors has been proposed previously in this system via the Notch signaling pathway ([Chapouton et al., 2010](#)).

The activity of the insulin and IGF signaling pathway is important in several developmental and regenerating

Figure 6. Overexpression of IGF2b Induces Complete Cell Division in Young Cells, but Incomplete Division in Old Cells

(A–P) Brains were lipofected *in vivo* 4 days prior to fixation with mtdTomato (control, A–D and I–L) or with mtdTomato and *igf2b* (IGF2b, E–H and M–P). Single confocal planes are displayed in the left panels and 3D reconstructions in the rightmost panels (D, H, L, and P). Cell nuclei (Hoechst, gray) and membrane labeling of the lipofected cells (magenta) are shown in (A), (E), (I), and (M). (A–D) Young control lipofected cells reveal infrequent cell division events, while young cells with IGF2b overexpression (E–H) reveal a higher incidence of cell division events, being visible as two neighboring cells immediately abutting each other (E–H, arrows). (M–P) Old control lipofected cells with IGF2b overexpression result in large cells with two nuclei, indicating an incomplete division (arrows in M, N, and P). (Q–W) Brains fixed 5 days after *igf2b* lipofection also reveal binucleated large cells (arrows in Q, R, and W), visible here in two distinct confocal planes (Q–S and T–V). Some neighboring cells reveal the same phenotype (arrowheads in Q, T, and U). (X) Cells having divided after lipofection were quantified in 6 experiments with a total of 69 young-control, 114 young-*igf2b*, 64 old-control, and 71 old-*igf2b* cells. The significance was calculated by a chi-squared test (young, *** $p = 0.7 \times 10^{-3}$; old, * $p = 0.01$). Scale bars, 10 μ m.



systems and shows multiple effects at distinct ages. These pathways are generally associated with nutrient sensing, growth, and metabolism, and play important roles in the homeostasis of NSCs (Rafalski and Brunet, 2011; Ziegler et al., 2015). IGF signaling induces proliferation and regulates the length of the cell cycle (Hodge et al., 2004; Mairet-Coello et al., 2009; Nieto-Estevez et al., 2016; Popken et al., 2004; Yuan et al., 2015), in some instances acting in combination with other growth factors, such as the EGFR (Alagappan et al., 2014). With age, systemic and brain levels of IGF ligands are reduced (Rafalski and Brunet, 2011; Shetty et al., 2005). These properties suggest that a maintained IGF pathway would be advantageous for counteracting an age-related proliferative decline. Indeed, infusion of IGF could restore higher levels of proliferation and neurogenesis in aged rats (Lichtenwalner et al., 2001). In contrast, most of the current literature suggests that inhibition of this pathway is beneficial for animals' longevity (Kappeler et al., 2008; Lopez-Otin et al., 2016), an effect also being observed in dwarf mutant mice (Sun, 2006). For instance, neurogenesis is maintained longer when IGF1R is conditionally deleted in the hypothalamus (Chaker et al., 2016) and SVZ (Chaker et al., 2015). Our results add a new aspect, as they show that NSCs lose their responsiveness to the IGF pathway with age. The reduction takes place both at the level of expression of the receptors and at the level of the proliferative response, remaining incomplete in old brains. Hence, we identify a cell-intrinsic change that might represent a protective response of cells. Collectively these observations lead to the concept that declining levels of neurogenesis with age could be, as opposed to a deficit, an actual benefit linked with healthy aging, whereby cells reduce at the same time their proliferative and general metabolic activity (see Hamilton et al., 2013). Thus, some of the changes observed with age might be the ones that promote longevity.

We have previously shown that aged radial glia are activated in lower percentage by an injury protocol than are young cells (Edelmann et al., 2013). Together with the results presented here, this indicates significant cell-intrinsic changes with age. It will be fundamental in the future to understand the respective contributions of cell-intrinsic changes and signals received from the neighborhood in order to understand under which conditions manipulations to rejuvenate aging tissue can be successful.

EXPERIMENTAL PROCEDURES

See Supplemental Information for details of all experimental procedures.

Animal Maintenance

Zebrafish were bred and maintained in the animal facility of the Helmholtz Zentrum München. Wild-type zebrafish (AB) or

the transgenic line *gfap:GFP* (Bernardos and Raymond, 2006) (mi2001) in the AB background were used. Animal experiments were conducted in accordance with the laws of the government of Oberbayern (animal protocol 55.2-1-54-2531-83-14).

Further information and requests for resources and reagents should be directed to and will be fulfilled by P.C. (chapouton@helmholtz-muenchen.de).

SUPPLEMENTAL INFORMATION

Supplemental Information includes Supplemental Experimental Procedures, seven figures, and six tables and can be found with this article online at <https://doi.org/10.1016/j.stemcr.2018.12.005>.

AUTHOR CONTRIBUTIONS

J.O. performed the gene ontology analysis, generated all graphs representing the proteomics dataset, and wrote the proteomics methods; F.W. produced the SFRP-EGFP construct; A.K. contributed to the FACS experiments; A.Z. performed the RNA-seq experiments on FACS isolated cells; J.N. analyzed the RNA-seq results; S.M.H. designed the biotinylation protocols and analyzed the mass spectrometry data; P.C. conceived the study, performed the experiments, prepared the figures, and wrote the manuscript.

ACKNOWLEDGMENTS

We are thankful to Leanne Godinho for providing several constructs and for critical reading of the manuscript, Christian Stigloher for helpful comments on the manuscript, Oriol Viader-Llagues and Reinhard Köster for providing pCS2-lifect-RFP constructs, and Steffen Scholpp for providing the pCS2-Wnt8-mcherry plasmid. We thank Ayla Schröder, Sebnem Akbas, and Kathrin Edelmann who performed experiments during their respective practical courses, and Jennifer Behler and Fabian Gruhn for technical help in S.M.H.'s lab. We thank Andreas Ettinger and Maria-Elena Torres-Padilla for access to their confocal microscope. We acknowledge the work of the animal keepers. This work was performed in the lab of Hernán Lopez-Schier. This work was supported by Deutsche Forschungsgemeinschaft grants (HA6014/2-2 and PR 1248/2-2) and by intramural funding from Helmholtz Zentrum München – GmbH, Germany, which is funded by the German Federal Ministry of Education and Research (BMBF) and the State of Bavaria.

Received: July 20, 2017

Revised: October 12, 2018

Accepted: December 11, 2018

Published: January 10, 2019

REFERENCES

- Adolf, B., Chapouton, P., Lam, C.S., Topp, S., Tannhauser, B., Strahle, U., Gotz, M., and Bally-Cuif, L. (2006). Conserved and acquired features of adult neurogenesis in the zebrafish telencephalon. *Dev. Biol.* 295, 278–293.
- Alagappan, D., Ziegler, A.N., Chidambaram, S., Min, J., Wood, T.L., and Levison, S.W. (2014). Insulin-like growth factor receptor



signaling is necessary for epidermal growth factor mediated proliferation of SVZ neural precursors in vitro following neonatal hypoxia-ischemia. *Front. Neurol.* 5, 79.

Alunni, A., and Bally-Cuif, L. (2016). A comparative view of regenerative neurogenesis in vertebrates. *Development* 143, 741–753.

Alunni, A., Krecsmarik, M., Bosco, A., Galant, S., Pan, L., Moens, C.B., and Bally-Cuif, L. (2013). Notch3 signaling gates cell cycle entry and limits neural stem cell amplification in the adult pallium. *Development* 140, 3335–3347.

Barbosa, J.S., Sanchez-Gonzalez, R., Di Giaimo, R., Baumgart, E.V., Theis, F.J., Gotz, M., and Ninkovic, J. (2015). Neurodevelopment. Live imaging of adult neural stem cell behavior in the intact and injured zebrafish brain. *Science* 348, 789–793.

Batiz, L.F., Castro, M.A., Burgos, P.V., Velasquez, Z.D., Munoz, R.I., Lafourcade, C.A., Troncoso-Escudero, P., and Wyneken, U. (2015). Exosomes as novel regulators of adult neurogenic niches. *Front. Cell Neurosci.* 9, 501.

Baumgart, E.V., Barbosa, J.S., Bally-Cuif, L., Gotz, M., and Ninkovic, J. (2012). Stab wound injury of the zebrafish telencephalon: a model for comparative analysis of reactive gliosis. *Glia* 60, 343–357.

Bernardos, R.L., and Raymond, P.A. (2006). GFAP transgenic zebrafish. *Gene Expr. Patterns* 6, 1007–1013.

Bracko, O., Singer, T., Aigner, S., Knobloch, M., Winner, B., Ray, J., Clemenson, G.D., Jr., Suh, H., Couillard-Despres, S., Aigner, L., et al. (2012). Gene expression profiling of neural stem cells and their neuronal progeny reveals IGF2 as a regulator of adult hippocampal neurogenesis. *J. Neurosci.* 32, 3376–3387.

Calzolari, F., Michel, J., Baumgart, E.V., Theis, F., Gotz, M., and Ninkovic, J. (2015). Fast clonal expansion and limited neural stem cell self-renewal in the adult subependymal zone. *Nat. Neurosci.* 18, 490–492.

Capilla-Gonzalez, V., Cebrian-Silla, A., Guerrero-Cazares, H., Garcia-Verdugo, J.M., and Quinones-Hinojosa, A. (2014). Age-related changes in astrocytic and ependymal cells of the subventricular zone. *Glia* 62, 790–803.

Carlen, M., Meletis, K., Goritz, C., Darsalia, V., Evergren, E., Tanigaki, K., Amendola, M., Barnabe-Heider, F., Yeung, M.S., Naldini, L., et al. (2009). Forebrain ependymal cells are Notch-dependent and generate neuroblasts and astrocytes after stroke. *Nat. Neurosci.* 12, 259–267.

Chaker, Z., Aid, S., Berry, H., and Holzenberger, M. (2015). Suppression of IGF-I signals in neural stem cells enhances neurogenesis and olfactory function during aging. *Aging Cell* 14, 847–856.

Chaker, Z., George, C., Petrovska, M., Caron, J.B., Lacube, P., Caille, I., and Holzenberger, M. (2016). Hypothalamic neurogenesis persists in the aging brain and is controlled by energy-sensing IGF-I pathway. *Neurobiol. Aging* 41, 64–72.

Chapouton, P., Skupien, P., Hesl, B., Coolen, M., Moore, J.C., Madelaine, R., Kremmer, E., Faus-Kessler, T., Blader, P., Lawson, N.D., et al. (2010). Notch activity levels control the balance between quiescence and recruitment of adult neural stem cells. *J. Neurosci.* 30, 7961–7974.

Cohen, M., Georgiou, M., Stevenson, N.L., Miodownik, M., and Baum, B. (2010). Dynamic filopodia transmit intermittent Delta-

Notch signaling to drive pattern refinement during lateral inhibition. *Dev. Cell* 19, 78–89.

Daynac, M., Morizur, L., Chicheportiche, A., Mouthon, M.A., and Boussin, F.D. (2016). Age-related neurogenesis decline in the subventricular zone is associated with specific cell cycle regulation changes in activated neural stem cells. *Sci. Rep.* 6, 21505.

Daynac, M., Pineda, J.R., Chicheportiche, A., Gauthier, L.R., Morizur, L., Boussin, F.D., and Mouthon, M.A. (2014). TGFbeta lengthens the G1 phase of stem cells in aged mouse brain. *Stem Cells* 32, 3257–3265.

Diotel, N., Rodriguez Viales, R., Armant, O., Marz, M., Ferg, M., Rastegar, S., and Strahle, U. (2015). Comprehensive expression map of transcription regulators in the adult zebrafish telencephalon reveals distinct neurogenic niches. *J. Comp. Neurol.* 523, 1202–1221.

Dray, N., Bedu, S., Vuillemin, N., Alunni, A., Coolen, M., Krecsmarik, M., Supatto, W., Beaurepaire, E., and Bally-Cuif, L. (2015). Large-scale live imaging of adult neural stem cells in their endogenous niche. *Development* 142, 3592–3600.

Edelmann, K., Glashauser, L., Sprungala, S., Hesl, B., Fritschle, M., Ninkovic, J., Godinho, L., and Chapouton, P. (2013). Increased radial glia quiescence, decreased reactivation upon injury and unaltered neuroblast behavior underlie decreased neurogenesis in the aging zebrafish telencephalon. *J. Comp. Neurol.* 521, 3099–3115.

Ehm, O., Goritz, C., Covic, M., Schaffner, I., Schwarz, T.J., Karaca, E., Kempkes, B., Kremmer, E., Pfrieger, F.W., Espinosa, L., et al. (2010). RBPJkappa-dependent signaling is essential for long-term maintenance of neural stem cells in the adult hippocampus. *J. Neurosci.* 30, 13794–13807.

Encinas, J.M., Michurina, T.V., Peunova, N., Park, J.H., Tordo, J., Peterson, D.A., Fishell, G., Koulakov, A., and Enikolopov, G. (2011). Division-coupled astrocytic differentiation and age-related depletion of neural stem cells in the adult hippocampus. *Cell Stem Cell* 8, 566–579.

Fuentealba, L.C., Obernier, K., and Alvarez-Buylla, A. (2012). Adult neural stem cells bridge their niche. *Cell Stem Cell* 10, 698–708.

Galant, S., Furlan, G., Coolen, M., Dirian, L., Foucher, I., and Bally-Cuif, L. (2016). Embryonic origin and lineage hierarchies of the neural progenitor subtypes building the zebrafish adult midbrain. *Dev. Biol.* 420, 120–135.

Ganz, J., Kaslin, J., Hochmann, S., Freudenreich, D., and Brand, M. (2010). Heterogeneity and Fgf dependence of adult neural progenitors in the zebrafish telencephalon. *Glia* 58, 1345–1363.

Goncalves, J.T., Schafer, S.T., and Gage, F.H. (2016). Adult neurogenesis in the hippocampus: from stem cells to behavior. *Cell* 167, 897–914.

Grandel, H., and Brand, M. (2013). Comparative aspects of adult neural stem cell activity in vertebrates. *Dev. Genes Evol.* 223, 131–147.

Grandel, H., Kaslin, J., Ganz, J., Wenzel, I., and Brand, M. (2006). Neural stem cells and neurogenesis in the adult zebrafish brain: origin, proliferation dynamics, migration and cell fate. *Dev. Biol.* 295, 263–277.

Grupp, L., Wolburg, H., and Mack, A.F. (2010). Astroglial structures in the zebrafish brain. *J. Comp. Neurol.* 518, 4277–4287.



- Hamilton, L.K., Joppe, S.E., M Cochard, L., and Fernandes, K.J. (2013). Aging and neurogenesis in the adult forebrain: what we have learned and where we should go from here. *Eur. J. Neurosci.* 37, 1978–1986.
- Hodge, R.D., D'Ercole, A.J., and O'Kusky, J.R. (2004). Insulin-like growth factor-I accelerates the cell cycle by decreasing G1 phase length and increases cell cycle reentry in the embryonic cerebral cortex. *J. Neurosci.* 24, 10201–10210.
- Hsieh, F.Y., Ma, T.L., Shih, H.Y., Lin, S.J., Huang, C.W., Wang, H.Y., and Cheng, Y.C. (2013). Dner inhibits neural progenitor proliferation and induces neuronal and glial differentiation in zebrafish. *Dev. Biol.* 375, 1–12.
- Kang, W., and Hebert, J.M. (2015). FGF signaling is necessary for neurogenesis in young mice and sufficient to reverse its decline in old mice. *J. Neurosci.* 35, 10217–10223.
- Kappeler, L., De Magalhaes Filho, C., Dupont, J., Leneuve, P., Cervera, P., Perin, L., Loudes, C., Blaise, A., Klein, R., Epelbaum, J., et al. (2008). Brain IGF-1 receptors control mammalian growth and lifespan through a neuroendocrine mechanism. *PLoS Biol.* 6, e254.
- Kaslin, J., Ganz, J., Geffarth, M., Grandel, H., Hans, S., and Brand, M. (2009). Stem cells in the adult zebrafish cerebellum: initiation and maintenance of a novel stem cell niche. *J. Neurosci.* 29, 6142–6153.
- Kaslin, J., Kroehne, V., Ganz, J., Hans, S., and Brand, M. (2017). Distinct roles of neuroepithelial-like and radial glia-like progenitor cells in cerebellar regeneration. *Development* 144, 1462–1471.
- Katz, S., Cussigh, D., Urban, N., Blomfield, I., Guillemot, F., Bally-Cuif, L., and Coolen, M. (2016). A nuclear role for miR-9 and argonaute proteins in balancing quiescent and activated neural stem cell states. *Cell Rep.* 17, 1383–1398.
- Kazanis, I., Lathia, J.D., Vadakkan, T.J., Raborn, E., Wan, R., Mughal, M.R., Eckley, D.M., Sasaki, T., Patton, B., Mattson, M.P., et al. (2010). Quiescence and activation of stem and precursor cell populations in the subependymal zone of the mammalian brain are associated with distinct cellular and extracellular matrix signals. *J. Neurosci.* 30, 9771–9781.
- Kroehne, V., Freudenreich, D., Hans, S., Kaslin, J., and Brand, M. (2011). Regeneration of the adult zebrafish brain from neurogenic radial glia-type progenitors. *Development* 138, 4831–4841.
- Kuhn, H.G., Dickinson-Anson, H., and Gage, F.H. (1996). Neurogenesis in the dentate gyrus of the adult rat: age-related decrease of neuronal progenitor proliferation. *J. Neurosci.* 16, 2027–2033.
- Lacar, B., Young, S.Z., Platel, J.C., and Bordey, A. (2011). Gap junction-mediated calcium waves define communication networks among murine postnatal neural progenitor cells. *Eur. J. Neurosci.* 34, 1895–1905.
- Lehtinen, M.K., Zappaterra, M.W., Chen, X., Yang, Y.J., Hill, A.D., Lun, M., Maynard, T., Gonzalez, D., Kim, S., Ye, P., et al. (2011). The cerebrospinal fluid provides a proliferative niche for neural progenitor cells. *Neuron* 69, 893–905.
- Lichtenwalner, R.J., Forbes, M.E., Bennett, S.A., Lynch, C.D., Sonntag, W.E., and Riddle, D.R. (2001). Intracerebroventricular infusion of insulin-like growth factor-I ameliorates the age-related decline in hippocampal neurogenesis. *Neuroscience* 107, 603–613.
- Lim, D.A., and Alvarez-Buylla, A. (2016). The adult ventricular-subventricular zone (V-SVZ) and olfactory bulb (OB) neurogenesis. *Cold Spring Harb. Perspect. Biol.* 8. <https://doi.org/10.1101/cshperspect.a018820>.
- Lopez-Otin, C., Galluzzi, L., Freije, J.M., Madeo, F., and Kroemer, G. (2016). Metabolic control of longevity. *Cell* 166, 802–821.
- Maggi, R., Zasso, J., and Conti, L. (2014). Neurodevelopmental origin and adult neurogenesis of the neuroendocrine hypothalamus. *Front. Cell Neurosci.* 8, 440.
- Mairet-Coello, G., Tury, A., and DiCicco-Bloom, E. (2009). Insulin-like growth factor-1 promotes G(1)/S cell cycle progression through bidirectional regulation of cyclins and cyclin-dependent kinase inhibitors via the phosphatidylinositol 3-kinase/Akt pathway in developing rat cerebral cortex. *J. Neurosci.* 29, 775–788.
- März, M., Chapouton, P., Diotel, N., Vaillant, C., Hesl, B., Takamiya, M., Lam, C.S., Kah, O., Bally-Cuif, L., and Strahle, U. (2010). Heterogeneity in progenitor cell subtypes in the ventricular zone of the zebrafish adult telencephalon. *Glia* 58, 870–888.
- Mirzadeh, Z., Merkle, F.T., Soriano-Navarro, M., Garcia-Verdugo, J.M., and Alvarez-Buylla, A. (2008). Neural stem cells confer unique pinwheel architecture to the ventricular surface in neurogenic regions of the adult brain. *Cell Stem Cell* 3, 265–278.
- Miura, Y., and Endo, T. (2016). Glycomics and glycoproteomics focused on aging and age-related diseases—glycans as a potential biomarker for physiological alterations. *Biochim. Biophys. Acta* 1860, 1608–1614.
- Nieto-Estevéz, V., Defterali, C., and Vicario-Abejon, C. (2016). IGF-I: a key growth factor that regulates neurogenesis and synaptogenesis from embryonic to adult stages of the brain. *Front. Neurosci.* 10, 52.
- Pastrana, E., Cheng, L.C., and Doetsch, F. (2009). Simultaneous prospective purification of adult subventricular zone neural stem cells and their progeny. *Proc. Natl. Acad. Sci. U S A* 106, 6387–6392.
- Popken, G.J., Hodge, R.D., Ye, P., Zhang, J., Ng, W., O'Kusky, J.R., and D'Ercole, A.J. (2004). In vivo effects of insulin-like growth factor-I (IGF-I) on prenatal and early postnatal development of the central nervous system. *Eur. J. Neurosci.* 19, 2056–2068.
- Porlan, E., Marti-Prado, B., Morante-Redolat, J.M., Consiglio, A., Delgado, A.C., Kypta, R., Lopez-Otin, C., Kirstein, M., and Farinas, I. (2014). MT5-MMP regulates adult neural stem cell functional quiescence through the cleavage of N-cadherin. *Nat. Cell Biol.* 16, 629–638.
- Prols, F., Sagar, and Scaal, M. (2016). Signaling filopodia in vertebrate embryonic development. *Cell Mol. Life Sci.* 73, 961–974.
- Rafalski, V.A., and Brunet, A. (2011). Energy metabolism in adult neural stem cell fate. *Prog. Neurobiol.* 93, 182–203.
- Recabal, A., Caprile, T., and Garcia-Robles, M.L.A. (2017). Hypothalamic neurogenesis as an adaptive metabolic mechanism. *Front. Neurosci.* 11, 190.
- Rothensaigner, I., Krecsmarik, M., Hayes, J.A., Bahn, B., Lepier, A., Fortin, G., Gotz, M., Jagasia, R., and Bally-Cuif, L. (2011). Clonal analysis by distinct viral vectors identifies bona fide neural stem cells in the adult zebrafish telencephalon and characterizes their division properties and fate. *Development* 138, 1459–1469.



- Schlueter, P.J., Royer, T., Farah, M.H., Laser, B., Chan, S.J., Steiner, D.F., and Duan, C. (2006). Gene duplication and functional divergence of the zebrafish insulin-like growth factor 1 receptors. *FASEB J.* 20, 1230–1232.
- Shetty, A.K., Hattiangady, B., and Shetty, G.A. (2005). Stem/progenitor cell proliferation factors FGF-2, IGF-1, and VEGF exhibit early decline during the course of aging in the hippocampus: role of astrocytes. *Glia* 51, 173–186.
- Stanganello, E., Hagemann, A.I., Mattes, B., Sinner, C., Meyen, D., Weber, S., Schug, A., Raz, E., and Scholpp, S. (2015). Filopodia-based Wnt transport during vertebrate tissue patterning. *Nat. Commun.* 6, 5846.
- Sun, L.Y. (2006). Hippocampal IGF-1 expression, neurogenesis and slowed aging: clues to longevity from mutant mice. *Age (Dordr)* 28, 181–189.
- Than-Trong, E., and Bally-Cuif, L. (2015). Radial glia and neural progenitors in the adult zebrafish central nervous system. *Glia* 63, 1406–1428.
- Villeda, S.A., Luo, J., Mosher, K.I., Zou, B., Britschgi, M., Bieri, G., Stan, T.M., Fainberg, N., Ding, Z., Eggel, A., et al. (2011). The ageing systemic milieu negatively regulates neurogenesis and cognitive function. *Nature* 477, 90–94.
- Wullimann, M.F., and Mueller, T. (2004). Teleostean and mammalian forebrains contrasted: evidence from genes to behavior. *J. Comp. Neurol.* 475, 143–162.
- Yamada, T., Kerever, A., Yoshimura, Y., Suzuki, Y., Nonaka, R., Higashi, K., Toida, T., Mercier, F., and Arikawa-Hirasawa, E. (2017). Heparan sulfate alterations in extracellular matrix structures and FGF-2 signaling impairment in the aged neurogenic niche. *J. Neurochem.* 142, 534–544.
- Yuan, H., Chen, R., Wu, L., Chen, Q., Hu, A., Zhang, T., Wang, Z., and Zhu, X. (2015). The regulatory mechanism of neurogenesis by IGF-1 in adult mice. *Mol. Neurobiol.* 51, 512–522.
- Ziegler, A.N., Levison, S.W., and Wood, T.L. (2015). Insulin and IGF receptor signalling in neural-stem-cell homeostasis. *Nat. Rev. Endocrinol.* 11, 161–170.

Stem Cell Reports, Volume 12

Supplemental Information

**The Surface Proteome of Adult Neural Stem Cells in Zebrafish Unveils
Long-Range Cell-Cell Connections and Age-Related Changes
in Responsiveness to IGF**

Jara Obermann, Felicia Wagner, Anita Kociaj, Alessandro Zambusi, Jovica Ninkovic, Stefanie M. Hauck, and Prisca Chapouton

Experimental procedures

Biotinylation of the zebrafish brain surface

a- Biotinylation via glycosyl side chains

Brains (3 replicates of 6 two-years-old; 3 replicates of 6 four-months-old brains) were dissected and incubated in 330µl biotinylation reagent (20 mM NaIO₄, 100 µM biotin (both Gentaur, Aachen, Germany) and 10 mM aniline (Sigma Aldrich, Deisenhofen, Germany) in PBS pH 6.7) in the dark for 30 minutes at 4°C. The reaction was quenched with 1mM glycerol for 5 minutes. Brains were dissected into dorsal (pallium) and ventral (subpallium) part, lysed in 100µl lysis buffer containing 1% NP-40, sonicated and centrifuged. The supernatant was incubated with 10µl washed streptavidin beads for two hours at 4°C and frozen at -20°C. Streptavidin beads were washed (with 500µl 1xTBS and with 500µl UC buffer (5M urea, 100mM Tris-HCl, pH8.5). Beads were incubated with 200µl UC buffer containing 100mM DTT for 30 minutes at room temperature, washed with 500µl UC buffer, incubated with 200µl UC buffer containing 50mM iodoacetamide for 30 minutes at room temperature, washed with 200µl UC buffer containing 100mM DTT, with 500µl 5M NaCl, with 500µl 100mM Na₂CO₃ (pH 11.5) and twice with 500µl 100mM Tris-HCl, pH 8.5). After digestion overnight at 37°C in 40µl 50 mM Tris-HCl, pH 8.5, containing 1µg trypsin (Promega, Mannheim, Germany) beads were centrifuged and the supernatant containing tryptic peptides was transferred to a new tube. Beads were resuspended once with 20µl 50 mM Tris-HCl, pH 8.5, centrifuged and the supernatant was pooled with the first tryptic fraction, centrifuged through FASP filter and acidified with TFA (pH2).

b- Biotinylation via amino groups

Biotinylation via amino groups was performed with a cell surface protein isolation kit (Thermo scientific 89881) coupling biotin on NH₂ residues via EZ-Link™ Sulfo-NHS-SS-Biotin labelling. Brains (3 replicates of 6x two-year-old brains; 3 replicates of 7x four-month-old brains) were dissected in cold PBS (-Ca²⁺;-Mg²⁺) and the hemispheres of the telencephalon gently pulled apart from each other in order to disrupt partly the tela choroida and allow for the penetration of the biotinylation reagent into the ventricle. The brains were incubated in 12 ml Sulfo-NHS-SS-Biotin reagent per tube for 30 minutes at 4°C and the biotinylation reaction stopped with 200µl quenching solution (50mM Glycine in PBS), brains were washed with TBS, and telencephalons dissected into dorsal (dorsal pallium) and ventral (subpallium) part, then collected in 500µl lysis buffer (provided by the kit).

The tissue was transferred to 2 ml Precellys tubes, containing 12 small ceramic and 3 big ceramic beads, and lysed in the tissue homogenizer Precellys. Cell lysates were centrifuged at 10,000 ×g for 10 minutes at 4°C and the clarified supernatant was frozen at -20°C. 50µL of the NeutrAvidin Agarose

slurry (provided by the kit) was added to each column, washed and clarified cell lysate was added to the gel. After incubation for 60 minutes at room temperature with end-over-end mixing and following centrifugation for 1 minute at 1000 ×g, flow-through (intracellular fraction) was collected in separate tubes and stored at -20°C with Protease inhibitors. 50µL sample buffer (62.5mM Tris HCl, pH 6.8, 1% SDS, 10% Glycerol) containing 50 mM DTT was added to the gel and mixed end-over-end for 60 minutes at room temperature. After centrifugation, eluates were collected and frozen at -20°C.

Mass spectrometry

The identification of the isolated proteins was performed by LC-MS mass spectrometry on an LTQ OrbitrapXL (Thermo Fisher Scientific Inc.) (Grosche et al. 2016), or on a Q Exactive HF (Thermo Fisher Scientific). Digested peptides were loaded automatically onto an Ultimate3000 nano HPLC system (Dionex, Sunnyvale, CA) equipped with a nanotrap column (300 µm inner diameter × 5 mm, packed with Acclaim PepMap100 C18, 5 µm, 100 Å; LC Packings, Sunnyvale, CA) at a flow rate of 30µl/min in HPLC buffer containing 0.1% trifluoroacetic acid (TFA) for 5 minutes.

Different concentrations of buffer A (LTQ OrbitrapXL: 5% ACN in 0.1% formic acid (FA); Q Exactive HF: 2% ACN in 0.1% FA) and buffer B (LTQ OrbitrapXL: 80% ACN in 0.1% FA; Q Exactive HF: 100% ACN in 0.1% FA) were used to separate the peptides by increasing ACN concentrations on a reversed phase chromatography (LTQ OrbitrapXL: 75 µm inner diameter x 15 cm, Acclaim PepMap100 C18, 3 µm, 100A, Dionex; Q Exactive H: AcquityMST3 column, 25 cm, 1.8 µm, Waters) over 120 (LTQ OrbitrapXL) or 130 (Q Exactive HF) minutes at a flow rate of 250 nl/min.

From the high resolution MS prescan the 10 most abundant peptide ions for fragmentation in the HCD cell were acquired.

Survey full scan MS spectra (from m/z 200 to 1500) were measured with high-resolution (60,000 full-width half maximum). Target peptides already selected for MS/MS were dynamically excluded for 30 seconds.

Label-free quantification

LC-MS/MS-derived MS/MS spectra were directly imported as raw files into Progenesis QI software for proteomics (Version 2.5, Nonlinear Dynamics, Waters, Newcastle upon Tyne, U.K.) and label-free quantification was performed as previously described (Grosche et al. 2016). Briefly, profile data of the MS scans as well as MS/MS spectra were transformed to peak lists with respective m/z values, intensities, m/z width and abundances. The most complex sample was set as a reference, and the retention times of all other samples within the experiment were aligned (3 to 5 manual landmarks, followed by automatic alignment) to create maximal overlay of the two-dimensional feature maps. Features with charge scores of one or above 7 were excluded from further analysis. Subsequently,

samples were grouped (young or old, respectively) and all features were normalized. Peptide identification was performed with Mascot (Matrix Science, Version 2.2.06) using the Ensembl zebrafish public database (genome assembly Zv9; http://www.ensembl.org/Danio_rerio/) and setting trypsin as digestion enzyme and allowing fragment ion mass tolerances of 0.6 Da (Orbitrap XL data) or 20mmu (Q Exactive HF data) and parent ion tolerances of 10 ppm. One missed cleavage was allowed and iodoacetamide derivatives of cysteines were set as stable modifications as well as oxidation of methionine and deamidation of asparagine and glutamine as variable modifications. A Mascot-integrated decoy database search calculated an average false discovery (FDR) of <1.2% when searches were performed with a mascot percolator score cut-off of 13 and an appropriate significance threshold p.

Peptide assignments were reimported into Progenesis Q1 and all normalized abundances of unique peptides of an identified protein are summed for the total cumulative normalized of the respective protein.

Gene Ontology (GO) and Phobius algorithm

Proteins identified by LC-MS/MS were analyzed for the presence of transmembrane domains and/or signal peptides by the Phobius algorithm based on the amino acid sequence of a protein (Käll et al. 2004). Identified proteins were also analyzed by the Genomatix (GO) software suite to determine their “cellular components” either directly from the entries in the zebrafish database or by searching orthologue entries in the human database. Proteins annotated with GO terms “extracellular region”, “membrane” and/or “plasma membrane” were considered as being potentially located on the cell surface in addition to those with transmembrane domains or secretion signal peptides.

List of proteins were examined for overrepresented signaling pathways in the Genomatix Generanker and GePS (Genomatix Pathway Sytem) analyses tools.

Statistical analysis

Normalized abundances of the identified proteins of young and aged neural stem cells were compared and proteins which were 2 fold up- or downregulated were accepted as differentially expressed. Proteins without unique peptides were excluded of the analysis. Normal distribution was assumed and significance was determined by Student’s t-test. Proteins with p-values lower than 0.05 were regarded as significantly changed.

Hierarchical clustering based on Euclidean distance and Principal Component analysis (PCA) was performed with Perseus (Tyanova et al. 2016) including log2 transformed normalized abundances of all identified proteins.

Plasmids

Igf1, *igf2a*, *igf2b*, *igf1Ra* and *igf1rb* were cloned from zebrafish embryonic cDNA into the Strataclone PCR cloning vector PSC-A for generation of antisense-RNA probes for in situ-hybridization, using the following primers: IGF1FW: 5' ATGTCTAGCGGTCATTTCTCCAGG 3'; IGF1R: 5' CTACATGCGATAGTTTCTGCCCCCT 3'; IGF2aFW: 5' ATGGATGATTACCATGTATTCTGTGCATC 3'; IGF2aR: 5' TCATTTTCGGGATGTGCTGATCTG.3' IGF2bFW: 5' ATGGAGGACCAACTAAAACATCATTCTGT 3'; IGF2bR: 5' TCACTTGTGGCTAACGTAGTTTCTGTG 3'; IGF1raFW: 5' CGAGGGATGTTTGGACCTATTTTG 3'; IGF1raR: 5' GACGAAGTCCACCTCGCTGGG 3'; IGF1rbFW: 5' AGCAAACAGAGGCGATATT 3'; IGF1rbR 5' GTGCACAACATGCTGACAGACACAC 3'. IGF2b was subcloned into pBH-5xuas with sma1 /Cla1 for use in Lipofections.

For lipofections (Supplementary information), EF1 α : gal4 was combined to 14xuas: MtdTomato and pBH 5x uas: IGF2b.

Further plasmids lipofected: pCS2-wnt8a-mcherry, pCS2-lynGFP, pCS2: FynRFP.

Sfrp1a was cloned from zebrafish embryonic cDNA and fused in 3' to EGFP in the pCDNA-EGFP vector using the Gibson cloning kit (NEB) using the following primers: FW-pCDNA3-sfrp1a:

GACCCAAGCTTGCCACCATGAAGTCCCTTGCATCTTTGTC; RV-Sfrp1a-Gly-egfp:

CCCTTGCTCACCATGCCCTTGAAGACATTCTCATAGGCAGG; FW- Gly-epfp:

GGCATGGTGAGCAAGGGCGAGG; RV-pCDNA3-stop-egfp:

CTATAGAATAGGGCCCTCTAGATTAGAATTCCTTGACAGCTCGTCCA. In order to enable zebrafish SFRP1-GFP to be secreted in the supernatant of mammalian cell lines the zebrafish specific signal peptide sequence was exchanged with a murine IgG kappa-leader sequence in pCR3-SFRP-GFP, using the following oligonucleotides and a Gibson cloning assembly: IgG-kappa-leader sequence:

ATGGAGACAGACACACTCCTGCTATGGGTACTGCTGCTCTGGGTTCAGGTTCCACTGGTGAC; IgG-kappa-

fw: AGGGAGACCCAAGCTTGCCACCATGGAGACAGACACACTCCTG; IgG-kappa-rv:

GCCAGCCATACTCAAATGTCTGGTCAACAGTGGAACTGGAAC; SFRP1.1_GFP-fw:

CAGACATTTGAGTATGGCTGGCC; SFRP1.1_GFP-rv: CATAGAAGGCGGCGGTGGAAT; SFRP1.2_GFP-fw:

TTCGAAATGACCGACCAAGC; SFRP1.2_GFP-rv: CATGGTGGCAAGCTTGGGT.

Lipofections *in vivo*

1.5 μ g of each plasmid in a total of 5 μ l dd Ambion H₂O was given to a solution containing 2 μ l of EBSS and 3 μ l of Lipofectamine 2000, briefly vortexed and incubated at room temperature for 20 minutes. Fish were anesthetized in 0.02 % MS222 and transferred into a wet foam piece. A thin whole was pierced into the skull by a thin needle (27G) and a small volume (less than 1 μ l) of lipofection solution was gently injected through a micro capillary into the brain ventricle by pressure injection, as previously described (Chapouton et al. 2010).

Transfection and expression of the SFRP1a-EGFP construct

6x10⁵ HEK 293T cells were seeded on 6-well plates in full medium and transfected the next day with 6 µg pCR3-IgGK-SFRP-GFP using Fugene HD transfection reagent (Promega) according to the manufacturer's instructions. 24h post transfection cells were washed with PBS and further cultured in FBS-free medium. The supernatant was harvested 48h post transfection.

In situ hybridisation

Brains were dissected and fixed in 4% Paraformaldehyde over night at 4°C. Gelatin albumin sections (100µm) were cut at the vibratome and in situ hybridization were performed using dig-labelled antisense RNA probes, as described in (Chapouton et al. 2011).

Immunohistochemistry

Dissected brains were fixed over-night in 4% PFA at 4°C, washed and embedded in 3% agarose. Vibratome sections (100µm) were prepared and blocked in 10% Normal goat serum with 0.5% Tritonx100. Immunohistochemistry was performed using following primary antibodies: Rabbit-anti Phospho-Tyr1161-IGF-1R, Assaybiotech A7114 (1:100) and Rabbit-anti-Phospho Akt (Ser473), Cell Signaling #9271 (1: 50), the Alexa 488-EGF complex, Thermo Fisher Scientific E13345 (1:1000) or the SFRP1a-GFP supernatant on floating vibratome sections in 24-well plates. Goat-anti-rabbit –Alexa561 or- Alexa633 (Thermo Fisher Scientific) were used at a dilution of 1:1000. Streptavidin-Alexa555 (Thermo Fisher Scientific) was diluted 1:1000.

Fluorescence Activated Cell Sorting (FACS) of adult neural stem cells

20 telencephalons per experiment were dissected in cold HBSS (Hank's balanced salt solution, Life Technologies, Cat. num. 24020). 5 telencephalons per tube were covered with 3 ml dissociation solution (10% (vol/vol) HBSS (Hank's balanced salt solution, Life Technologies, Cat. num. 24020), 1,8% (vol/vol) D-(+)- glucose (SIGMA®, Cat. num. G8769), 1,5% (vol/vol) HEPES (Life Technologies, Cat. num. 15630-080), 0.002% Trypsin-EDTA (Life Technologies, Cat. Num. 25300-054), pH 7.5). The tissue and cells were dissociated for 20 min at 30°C. After 10 min the tissue was mechanically dissociated with a fire-polished, medium coated Pasteur pipette and incubated for additional 10 min. The enzymatic reaction was stopped with 3ml of stop solution (2% (vol/vol) HEPES (Life Technologies, Cat. num. 15630-080), 4% (wt/vol) Bovine serum albumin (SIGMA-ALDRICH®, Cat. num. [A4503](#)) and EBSS (Earle's Balanced Salt Solution) (Life technologies, Cat. num. [14155063](#)). The cell suspension was filtered through a 70 µm strainer and centrifuged for 7 min at 1500 rpm/min. The pellet was washed twice with 500 µl of Dulbecco's Phosphate Buffered saline (Life Technologies, Cat. num. 14190-094), filtered again, resuspended into 2ml PBS and sorted at the FACSaria III Cell Sorter (BD). Sorting gates

were set according to the WT tissue expressing no fluorescent marker and neural stem cells were sorted according to the GFP levels. Cellular debris were eliminated based on the positivity for propidium iodide. After the sorting, cells were centrifuged for 7min at 1500 rpm/min and either immediately stored at -80°C for protein extraction or plated on poly-D-lysine coated coverslips for fixation and image acquisition. 4 replicates containing 50.000 to 100.000 cells each (respectively GFP-positive and GFP-negative cells) were lysed and analyzed by mass spectrometry.

For RNA isolation, cells were directly sorted into extraction buffer and total RNA was isolated using the PicoPure RNA isolation kit, according to the manufacturer's instructions (Thermo Fisher Scientific).

Libraries for deep sequencing of FACS sorted cells

The quality and concentration of RNA was assessed on Agilent 2100 Bioanalyzer. Only RNA with RIN value higher than 8 were used for libraries preparation. cDNA was synthesized from 1ng of total RNA using SMART-Seq v4 Ultra Low Input RNA kit for Sequencing (Clontech), according to the manufacturer's instructions. The quality and concentration of cDNA was assessed on Agilent 2100 Bioanalyzer before proceeding to library preparation using MicroPlex Library Preparation kit v2 (Diagenode). All libraries (minimum of 3 biological replicates per condition) were processed together to minimize batch effects. Final libraries were evaluated and quantified using an Agilent 2100 Bioanalyzer and the concentration was measured additionally with Quant-iT PicoGreen dsDNA Assay Kit (Thermo Fisher Scientific) before sequencing. The uniquely barcoded libraries were multiplexed onto one lane and 50-bp paired-end deep sequencing was carried out on HiSeq 4000 (Illumina) that generated approximately 20 million reads per sample.

The Kallisto pipeline (Bray et al. 2016) was then used to quantify the expression of transcripts. The Sleuth pipeline (Pimentel et al. 2017) was used for the statistical analysis. For the quantification, we aligned 30-kmers of 150 bp reads to the zebrafish Zv9 transcriptome containing both protein coding and non-coding genome using 100 bootstraps for every biological replicate (4 in total for each population). The most expressed isoform of gene was then used to generate the heatmap. The data in the heatmap (mean value of the replicates) is shown as log₂ of transcript per million.

Image acquisition and analysis

Vibratome sections or whole-mount brains were mounted in Vectashield (Vector Laboratories). Pictures were taken at the Leica SP5 or SP6 inverted confocal microscopes with the 63x glycerol immersion and 20x immersion objectives. In situ Hybridizations pictures were taken at the Zeiss axioplan with a matrix meteor video camera.

Confocal pictures were analyzed with ImageJ (Fiji). Filopodia were measured using the simple neurite tracer plugin. Mean fluorescence intensities were measured on manually defined ROIs (the whole cell soma in 3 different z-planes) on images taken with a hybrid detector. The 3D-viewer plugin was used to visualize all sides of the cells. Stackreg plugin was employed in case of deviation during z-stack acquisition (P. Thévenaz, U.E. Ruttimann, M. Unser A Pyramid Approach to Subpixel Registration Based on Intensity IEEE Transactions on Image Processing vol. 7, no. 1, pp. 27-41, January 1998).

Figures preparation

Figures were prepared in Adobe InDesign. Venn Diagramms were made with the Venny open source tool: <http://bioinfogp.cnb.csic.es/tools/venny/>, or with the Genomatix software. Graphs were prepared in Excel, Perseus (version 1.5.3.2; Computational Systems Biochemistry, Germany) and R Studio (RStudio Team (2015). RStudio: Integrated Development for R. RStudio, Inc., Boston, MA URL <http://www.rstudio.com/>) with the ggplot2 package.

References in the Supplementary Material:

- Bray NL, Pimentel H, Melsted P, Pachter L. 2016. Near-optimal probabilistic RNA-seq quantification. *Nat Biotechnol* **34**: 525-527.
- Chapouton P, Skupien P, Hesl B, Coolen M, Moore JC, Madelaine R, Kremmer E, Faus-Kessler T, Blader P, Lawson ND et al. 2010. Notch activity levels control the balance between quiescence and recruitment of adult neural stem cells. *J Neurosci* **30**: 7961-7974.
- Chapouton P, Webb KJ, Stigloher C, Alunni A, Adolf B, Hesl B, Topp S, Kremmer E, Bally-Cuif L. 2011. Expression of hairy/enhancer of split genes in neural progenitors and neurogenesis domains of the adult zebrafish brain. *J Comp Neurol* **519**: 1748-1769.
- Grosche A, Hauser A, Lepper MF, Mayo R, von Toerne C, Merl-Pham J, Hauck SM. 2016. The Proteome of Native Adult Muller Glial Cells From Murine Retina. *Molecular & cellular proteomics : MCP* **15**: 462-480.
- Käll L, Krogh A, Sonnhammer EL. 2004. A combined transmembrane topology and signal peptide prediction method. *Journal of molecular biology* **338**: 1027-1036.
- Pimentel H, Bray NL, Puente S, Melsted P, Pachter L. 2017. Differential analysis of RNA-seq incorporating quantification uncertainty. *Nat Methods* **14**: 687-690.
- Tyanova S, Temu T, Sinitcyn P, Carlson A, Hein MY, Geiger T, Mann M, Cox J. 2016. The Perseus computational platform for comprehensive analysis of (prote) omics data. *Nature methods* **13**: 731-740.

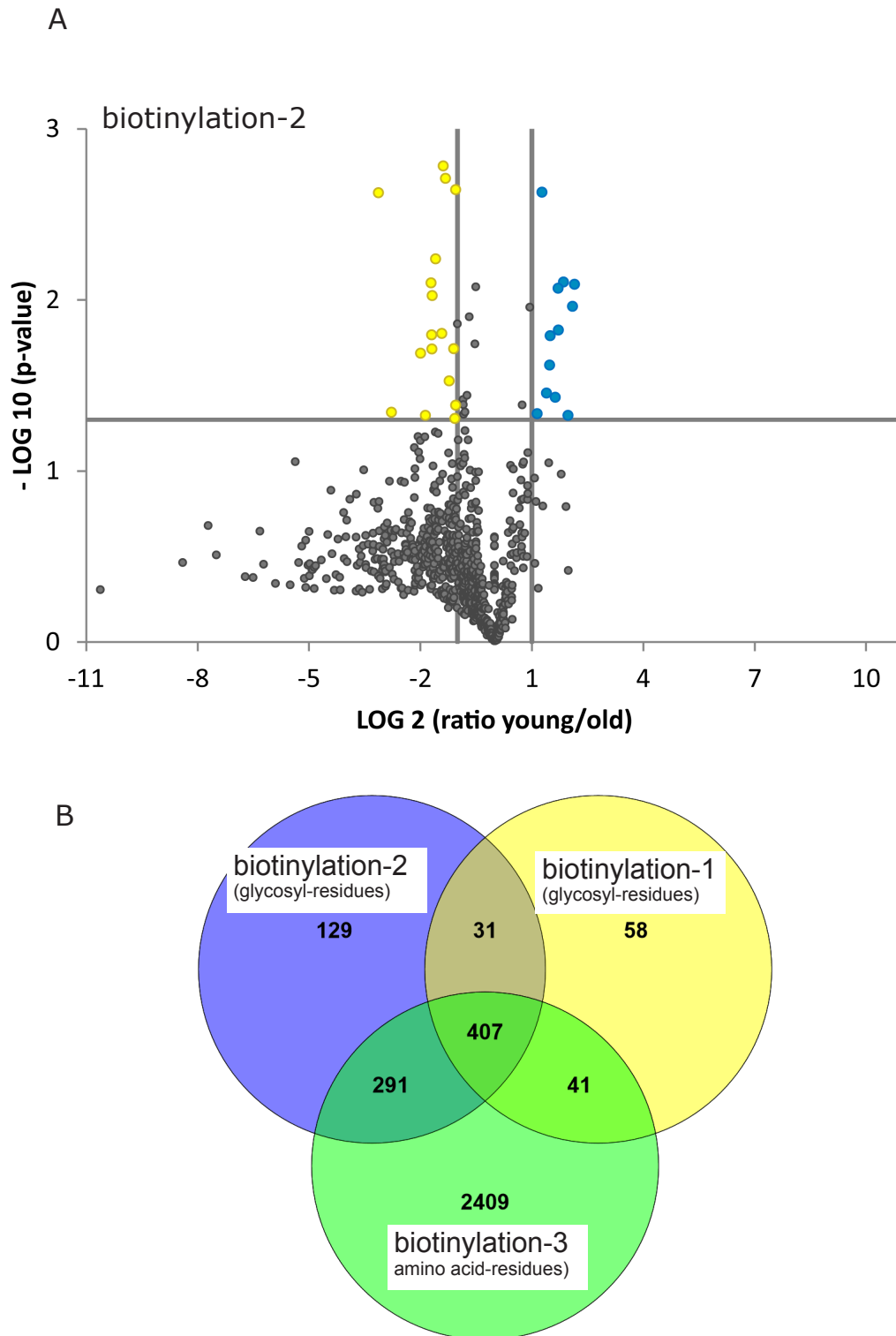


Figure S1: Proteins retrieved by two different biotinylation protocols

A: Volcano plot representation of the proteins identified by the glycosylation-dependent biotinylation, depicting young versus old ratios. Note the bias towards proteins with increased expression in aged brains (left side). B: Venn diagram of three experiments. The majority of proteins identified by the glycosylation-dependent biotinylations (1 and 2) are also identified in the amino-acid bound biotinylation (3). A higher number of proteins were identified in the latter approach.

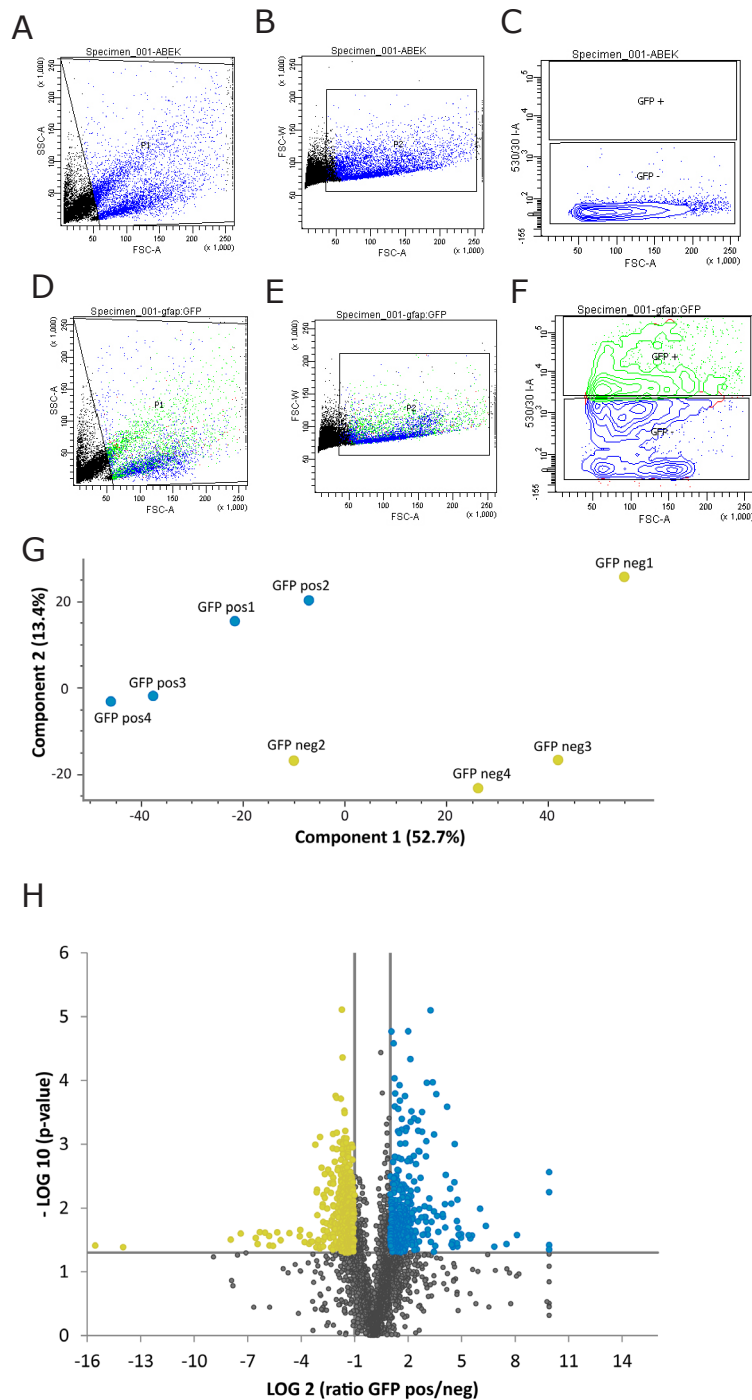


Figure S2: FACS isolation of cells and protein identification thereafter

A-F: dissociated cells were selected by forward scatter (FSC-A) and side scatter (SSC-A), P1 gate. B, E: Cellular aggregates are excluded on FSC-W and FSC-A gate, (P2). C: Gates for gfap:GFP sorting were based on AB wild-type zebrafish, which are negative for GFP. F: Plot depicting cells which do not express (GFP-negative gate) and cells that express GFP (GFP-positive gate). G: principal component analysis of the proteins identified in consecutive sorting experiments, depicting a consistent clustering of the fractions. H: volcano plot of the proteins upregulated in the GFP-positive fraction versus proteins upregulated in the GFP-negative fraction, revealing similar number of proteins on both sides.

Obermann et al., **Figure S3:**
Filopodia on radial glia in 2-year-old telencephalons.

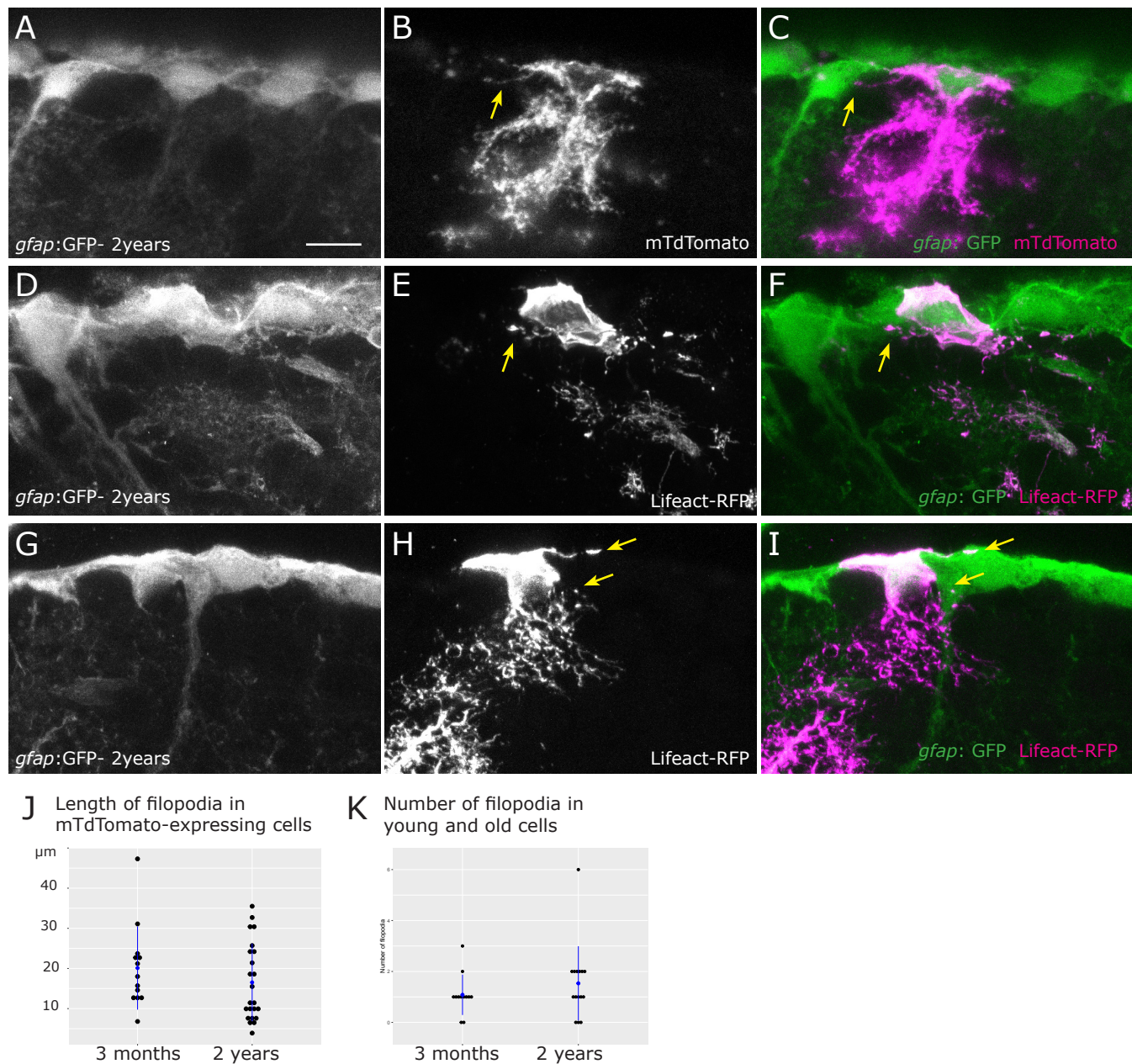
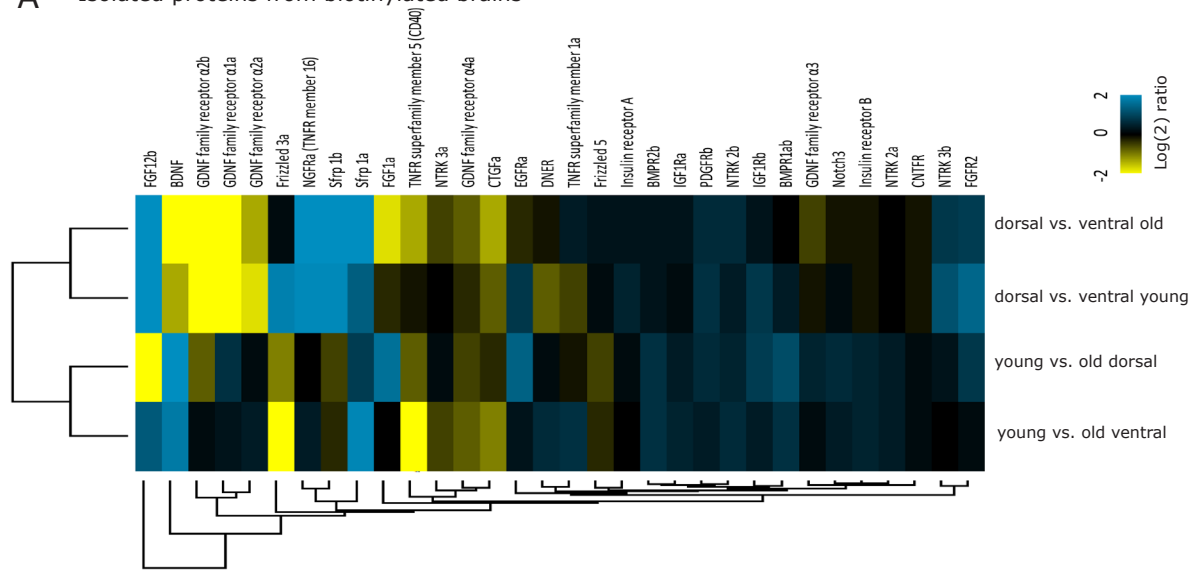


Figure S3: Filopodia on 2-year-old telencephalons.
2-year-old *gfap:GFP* brains lipofected with membrane bound mTdTomato (A-C) or with Lifeact-RFP (G-I) reveal the presence of filopodia on radial glia with similar sizes and similar numbers as in young brains. J, K: The length and number of filopodia was measured on cells lipofected with a membrane-localized construct (MTdTomato) (3-months and 2-years-old, 15 and 26 cells, respectively) and did not reveal significant differences (T: Mann-Withney test, $p=0.42$; U: Mann-Withney test, $p=0.36$).

Obermann et al., **Figure S4**: Surface receptors and ligands isolated as proteins in the biotinylated fraction and as RNA in FACS-sorted cells

A Isolated proteins from biotinylated brains



B RNA-seq data on FACS-sorted cells

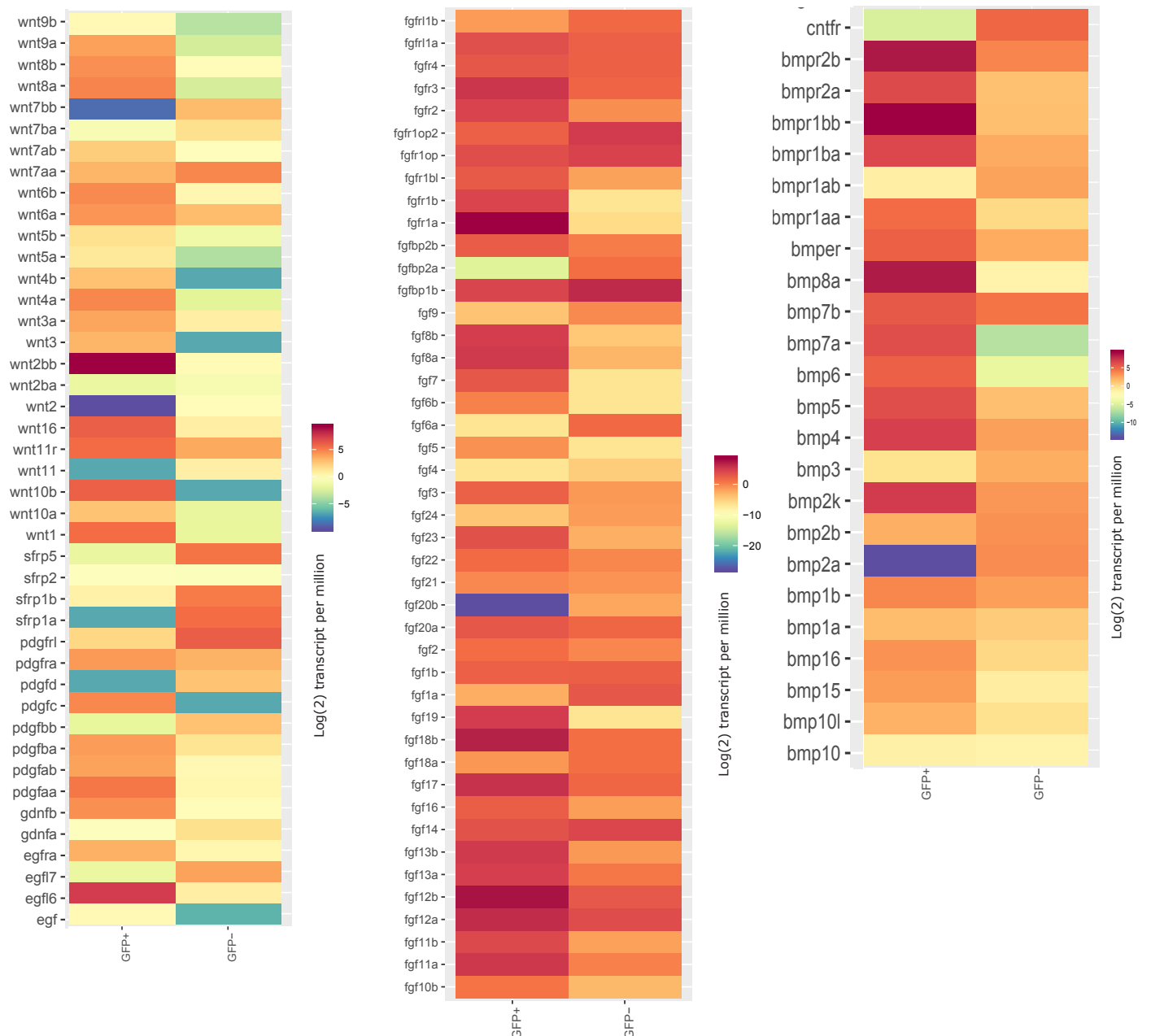


Figure S4: Surface receptor and ligands isolated as proteins in the biotinylated fraction and as RNA in FACS-sorted cells.

A: Surface receptors, as well as some ligands were clustered. Log (2) ratios of the expression levels are depicted. B: cDNA produced from sorted gfap:GFP-positive and -negative cells was sequenced and quantified. Members of the Wnt, PDGF, EGF, FGF, CNTF and BMP signal pathways are represented as log(2) transcripts per million.

Neither Wnt nor EGF signaling co-localize with filopodial extensions of adult radial glia

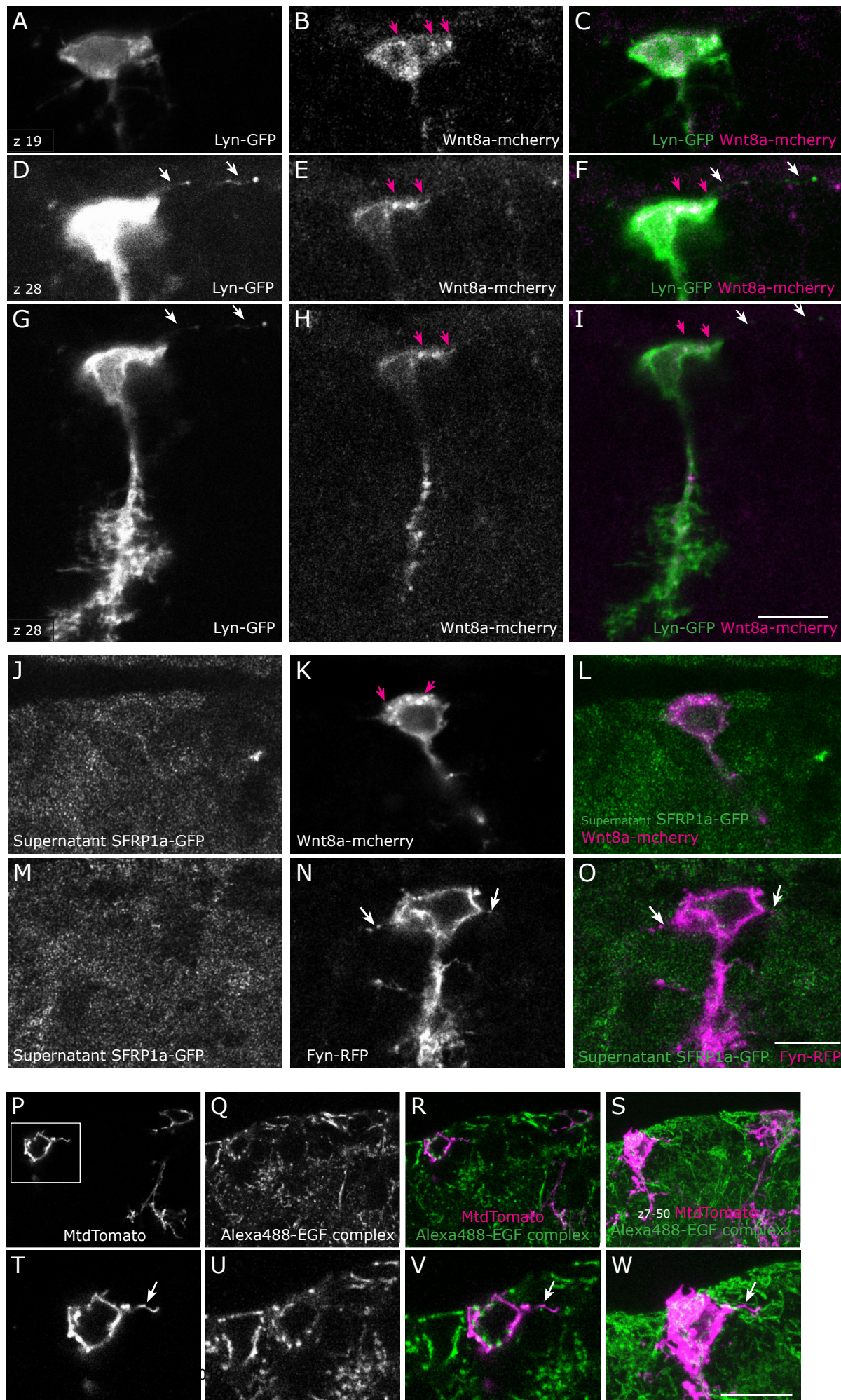


Figure S5: Neither Wnt nor EGF signaling co-localizes with filopodial extensions in adult radial glia.

A-I: Example of a cell in a 3-months-old wild-type (AB) brain co-lipofected with pCS2-lyn-GFP and pCS2-wnt8a-mcherry as single confocal planes (z19 in A-C and z28 in D-I). Wnt8a-mcherry localizes in a non-homogeneous manner in the radial glia and can be found at edges of the cytoplasm (pink arrows), however it does not localize in thin filopodial extensions labelled by Lyn-GFP (white arrows). Number of cells analyzed: 8. J-O: The supernatant of Hek-293 cells transfected with sfrp1a-GFP was applied on brain sections containing cells lipofected with pCS2-Wnt8a-mcherry (J-L), or with pCS2-fyn-RFP (M-O). The SFRP-GFP protein does not co-localize strongly with Wnt8a-mCherry (pink arrows in K), and does not co-localize with filopodia visible on Fyn-RFP-transfected cells (white arrows in N, O). Number of cells analyzed: 8. P: Staining of a 3-month-old wild-type brain section with the Alexa Fluor 488-EGF complex, which binds to the EGF receptor. Two lipofected cells are visible as a single confocal plane in P-R and as a maximum intensity projection in S. T-W: higher magnification of the inset region depicted in P showing the soma and a filopodial extension (arrow). The EGF-Alexa-488 complex does not co-localize with filopodial extensions. Number of cells analyzed: 12. Scale bars: 10µm.

Obermann et al., **Figure S6:**

Expression of *igf1*, *igf2a* and *-2b*, *igf1ra* and *igf1rb* in the adult telencephalon

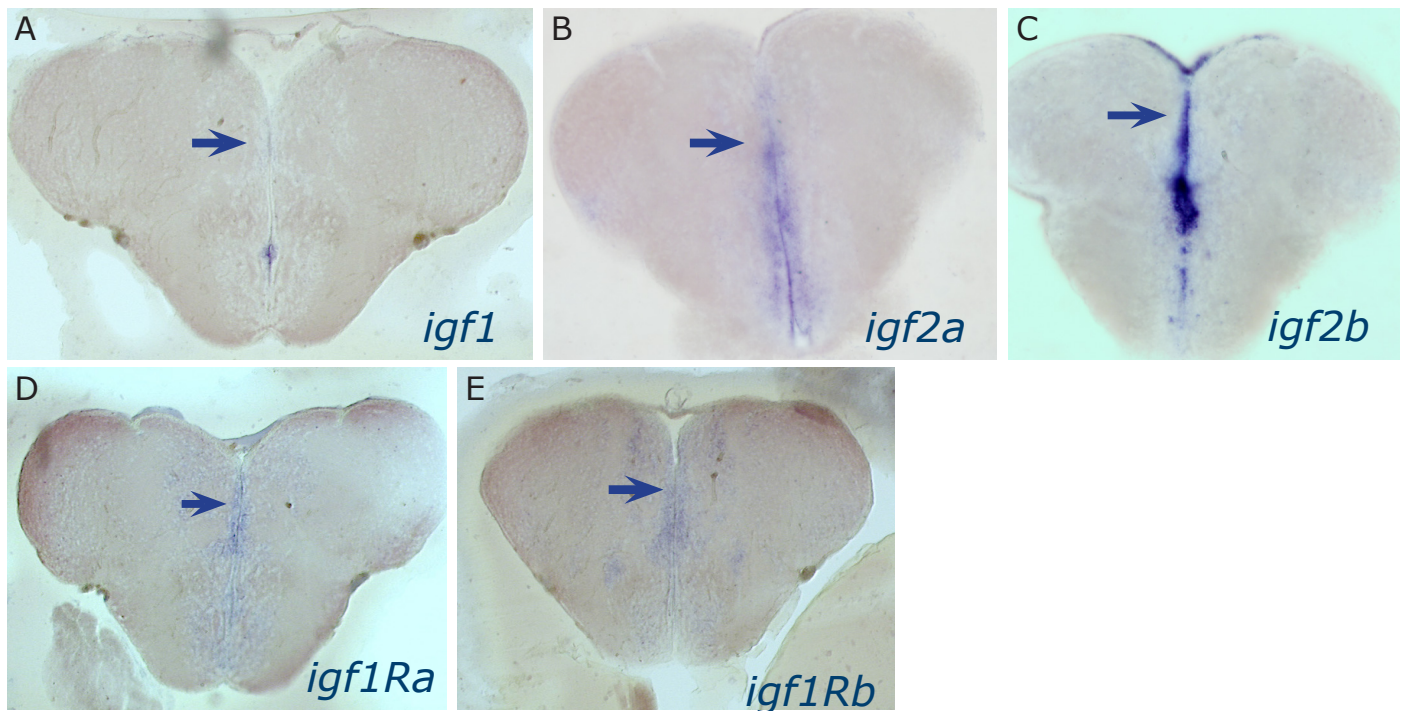


Figure S6: Expression of *igf 1*, *igf2a*, *igf2b*, *igf1ra* and *igf1rb* in the adult telencephalon.

In situ hybridization was performed on gelatin-albumine frontal sections of adult brains, with antisense probes as indicated in the panels. Expression is detected in the telencephalic ventricular zone (with a stronger expression level in the midline compared to the dorsal surface, where the signal was difficult to detect).

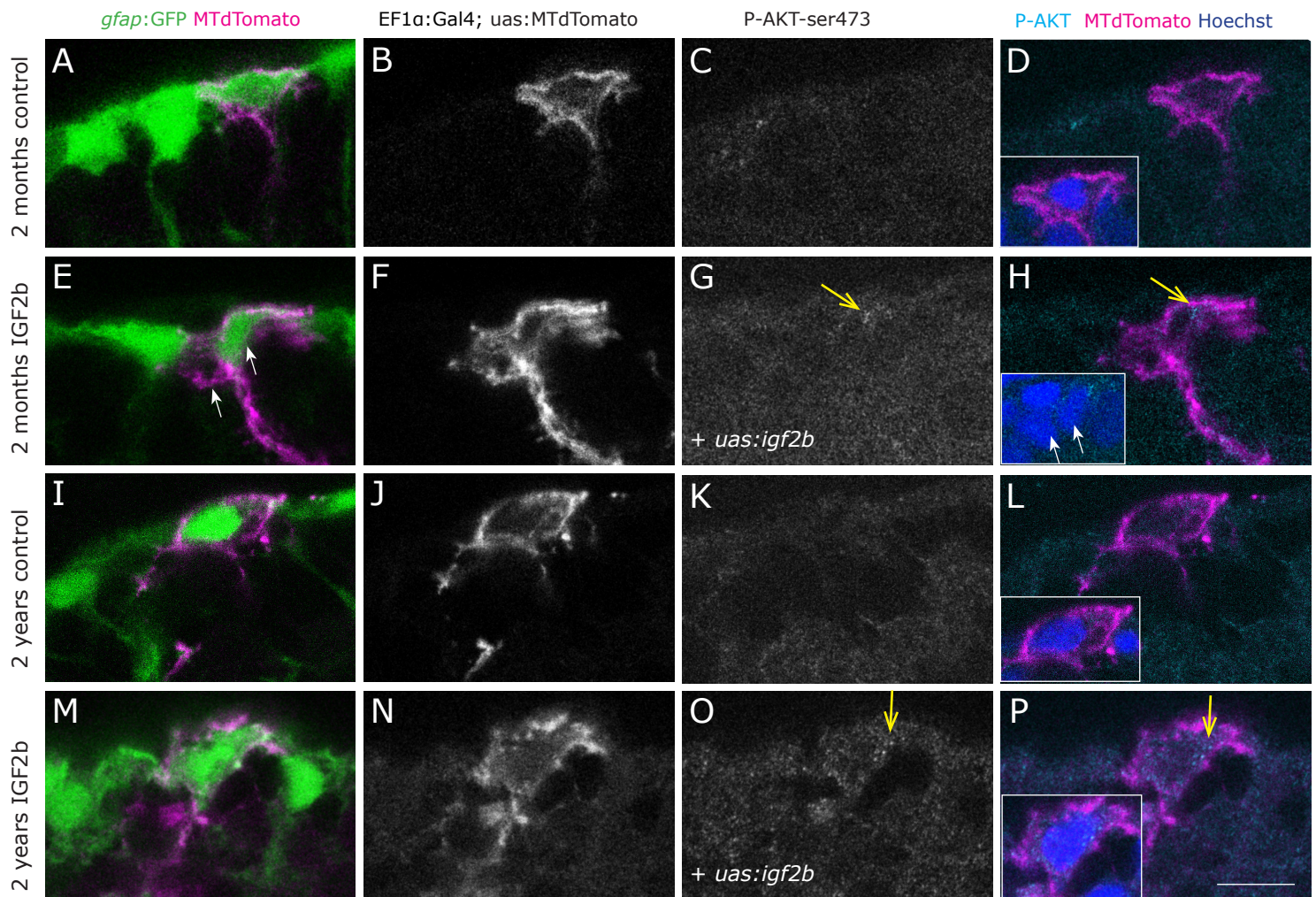


Figure S7: IGF2b overexpression reveals a moderate increase of phospho-Akt immunostaining.

Phosphorylated-AKT (Ser473) immunohistochemistry on young (A-H) and old (I-P) brains as a close-up view on the ventricular surface of the pallium. The radial glia somata, located at the border of the ventricle, are labelled in green by the *gfap:GFP* transgenic line. Single cells stained in magenta have been lipofected in vivo 4 days prior to brain fixation with MTdTomato (control, A-D; I-L) or with MTdTomato and *igf2b* (IGF2b, E-H; M-P) and are depicted as single confocal plane, highlighting primarily the cell soma (the radial process is not always in the plane of the optical section, therefore not always visible, but it is present below all the somata of lipofected cells). Dots of expression of P-Akt are visible in IGF2b lipofected cells (arrows in G, H, O, P). Insets in D, H, L and P are higher magnifications of the lipofected cells, the nuclei in blue are stained by DAPI. Single confocal planes are displayed, examples are taken out of 3 brains for each condition. Scale bar: 10µm

Table S1a:**Proteins identified in the FACS-GFP-positive fraction: overrepresented pathways**

Canonical pathway	P-value	List of observed genes
PDGFR-beta signaling pathway	2,57E-03	PPP2R2B, ACTR2, PRKCE, CYFIP2, MAPK10, ACTN4, NCKAP1, PRKCD
S1P4 pathway	2,58E-03	GNAI2, GNAO1, CDC42
attenuation of gpcr signaling	2,58E-03	GNAS, PRKAR2A, ARRB1
y branching of actin filaments	3,85E-03	ACTR2, CDC42, NCKAP1
N-cadherin signaling events	4,78E-03	CDC42, GSN, CTNNA1, GJA1
oxidative stress induced gene expression via nrf2	5,45E-03	POR, AKR7A2, CRYZ
Noncanonical Wnt signaling pathway	6,38E-03	CDC42, GNAS, CAMK2A
E-cadherin signaling in the nascent adherens junction	6,50E-03	CYFIP2, CDC42, CTNNA1, NCKAP1
Endothelins	7,25E-03	PRKCE, GNAI2, GNAO1, GNAS, PRKCD
phosphoinositides and their downstream targets	8,50E-03	GSK3B, PRKCE, PFKL
Stabilization and expansion of the E-cadherin adherens junction	8,50E-03	CYFIP2, CTNNA1, NCKAP1

Pathway	P-value	List of observed genes
REDOX	3,64E-08	PRDX6, GLUD1, GCDH, MIEN1, ACADS, POR, TXN2, CAT, GSPT1, GLRX3, GPD1L, LANCL1, FDXR, PRDX1, ACOX1, SRM, NNT, SCP2, GOT1, CTH
METABOTROPIC GLUTAMATE RECEPTOR	1,12E-04	GFAP, SLC6A1, SLC1A3, GRM2, MAPK10, SLC1A2, GLUL, SUCLG1, SLC17A6, HSPD1, GRM3
STRESS	1,65E-04	PRDX6, GCDH, SLC25A5, TXN2, AKR7A2, CAT, TRAP1, SDHA, IDH3A, BLVRA, PRDX1, ACOX1, SRM, CLTC, FAM213A, TPM3, ACO2
TRAFFICKING	2,07E-04	RAB14, CLTCL1, SNX6, ACTR2, SLC6A1, RTN3, MUT, PACSIN3, VWF, RALB, ENOSF1, RAB27B, FLOT2, SLC1A2, AAK1, RAB3A, SCP2, S100B, APPL1, SUCLG1, VPS35, PLP1, GJA1, TPM3, RAB10, SNAP91, DCTN4, ARRB1
CAVEOLIN 1	2,08E-04	PRKCE, ATIC, FLOT2, SLC1A2, PRDX1, CLTC, SCP2, GJA1, SNAP91
NITRIC OXIDE	3,38E-04	DLD, SLC32A1, CAT, VWF, GLUL, RGN, S100B, CTH, ACO1, ACO2, ADH5
INSULIN	3,95E-04	PDHA1, ATIC, EPHX1, FASN, ACLY, APPL2, SYP, ADD3, PSAT1, BLVRA, HK1, ACOT7, CTCF, RAB3A, SUCLA2, APPL1, NDUFV1
ENDOCYTIC	4,64E-04	RAB14, SYNJ1, SNX6, AP2B1, ACTR2, RBSN, SYP, AAK1, CDC42, CLTC, VTA1, MAPK8IP3, RAB3A, ATP6V1H, APPL1, VPS45, SNAP91, ARRB1
NITRIC OXIDE SYNTHASE	7,31E-04	DLD, ATIC, CAT, IDH3A, CRAT, BLVRA, AGMAT, RGN, CTH, ADH5

PROTEIN KINASE C	8,20E-04	SUCLG2, SLC8A1, SLC6A1, SLC1A3, PRKCE, PCYT2, VWF, GLRX3, CSPG5, RALB, GPD1L, SLC1A2, NDUFS2, GPM6A, S100B, SYT1, GJA1, ACO1, ACO2, PRKCD
AMYLOID BETA (A4) PRECURSOR PROTEIN	9,29E-04	SNX6, GFAP, GSK3B, GNAI2, SYP, ADD3, DPYSL2, S100B, CAMK2A
GLUTAMATE RECEPTOR, IONOTROPIC, N METHYL D ASPARTATE	1,17E-03	GLUD1, DLD, SLC1A3, BDNF, SLC17A6, CAMK2A, TPM3
CALCIUM/CALMODULIN DEPENDENT PROTEIN KINASE	1,50E-03	CAMK1D, SLC6A1, SLC1A3, NCAM1, BDNF, SYP, CLIC4, EEF2, SYT1, SLC17A6, CAMK2A, RAB10
ADP RIBOSYLATION FACTOR 1	2,66E-03	ACTR2, CYFIP2, ARHGAP1, CDC42, CYTH1
CANNABINOID RECEPTOR 1 (BRAIN)	4,21E-03	DLD, SLC32A1, GRM2, MGLL, ARRB1
ARRESTIN	4,85E-03	AP2B1, MAPK10, SUCLG1, PLP1, ARRB1
INOSITOL 1,4,5 TRIPHOSPHATE RECEPTOR, TYPE 1	5,91E-03	CA8, SYP, CDC42, GJA1
GLIAL CELL LINE DERIVED NEUROTROPHIC FACTOR (GDNF)	6,58E-03	SLC1A3, NCAM1, BDNF, SLC1A2, RAB3A, ACO1
LYSOPHOSPHATIDIC ACID RECEPTOR	7,00E-03	PRDX6, GSN, APPL1, SUCLG1
SECRETORY	7,52E-03	RTN3, VWF, SCAMP1, RAB27B, SYP, SCAMP3, SRM, AAK1, RTN1, RAB3A, CYTH1, SCP2, GNAS, VPS35, PLP1, GJA1, VPS45, PI4KA, HSPD1, STOM
ARP2 ACTIN RELATED PROTEIN 2 HOMOLOG (YEAST)	9,62E-03	ACTR2, WASF3, ARHGAP1, CDC42, GSN
CALCIUM	9,97E-03	CACNA2D2, CA8, PPM1K, VSNL1, SLC8A1, GFAP, RBSN, SLC6A1, VWF, SCAMP1, ATP1B1, ABAT, RGN, EEF2, PDZD11, S100B, SUCLG1, CAMK2A, ALDH5A1, ATP2B1

Table S1b:

Proteins identified in the FACS- GFP-negative fraction: overrepresented pathways

Canonical pathway	P-value	List of observed genes
spliceosomal assembly	1,76E-05	SNRPA1, SNRPC, SNRNP70, SNRPA
mechanism of protein import into the nucleus	1,16E-04	NUP153, RANBP1, NUP210, KPNB1
cycling of ran in nucleocytoplasmic transport	2,26E-04	NUP153, RANBP1, NUP210, XPO7
the information processing pathway at the ifn beta enhancer	4,52E-04	HMGB1, SMARCC1, GTF2F1, SMARCC2, TAF15, TAF12
chromatin remodeling by hswi/snf atp-dependent complexes	5,37E-04	SMARCC1, GTF2F1, SMARCC2, TAF15, TAF12
antisense pathway	3,10E-03	NONO, SFPQ
nuclear receptors coordinate the activities of chromatin remodeling complexes and coactivators to facilitate initiation of transcription in carcinoma cells	4,11E-03	NCOR2, GTF2F1, TAF15, TAF12

Signaling events mediated by HDAC Class I	6,82E-03	NUP153, GATAD2B, NCOR2, SIRT2, NUP210, SAP18
sumoylation by ranbp2 regulates transcriptional repression	8,92E-03	NUP153, NUP210, XPO7
proteasome complex	9,93E-03	PSMD14, PSME3, PSMB2, PSMA5

Pathway	P-value	List of observed genes
KH DOMAIN CONTAINING, RNA BINDING, SIGNAL TRANSDUCTION ASSOCIATED (SAM68)	6,78E-06	EWSR1, KHDRBS1, KHDRBS3, KHDRBS2, SRSF1, FBL, HNRNPK
SERINE/ARGININE SPLICING FACTOR PROTEIN KINASE	3,42E-05	SRSF10, SF1, PNN, SNRNP70, SRSF1, LBR
CELL DIVISION CYCLE 2, G1 TO S AND G2 TO M	3,77E-05	NPM1, CDC5L, RPS3, LMNA, EEF1D, GOLGA2, HMGB3, LMNB1, ENSA, SIRT2, FKBP2, SEPT9, AKAP8L, SRSF1, ELAVL1, LBR, TPR
CASEIN KINASE 2	4,56E-05	NPM1, RPS14, ANP32B, EEF1D, EIF5A, CBX5, HNRNPC, NCOR2, GTF2F1, PLS3, SSB, SUB1, RPL6, DEK, CBX1, RPS5, PRPF3, EIF1, HNRNPK
SET NUCLEAR ONCOGENE	5,87E-05	NPM1, BANF1, ANP32A, SET
SALT INDUCIBLE KINASE	5,14E-04	KHDRBS1, NUP93, CREB1, KHDRBS3, BANF1, KHDRBS2
CELL CYCLE	9,75E-04	NPM1, CDC5L, KHDRBS1, LMNA, RANBP1, RPS19, CBX5, HMGB3, SF3B1, LMNB1, GTF2F1, TAF15, NFYC, SIRT2, NUP210, VRK1, BANF1, CBX1, SART1, TIAL1, RUVBL1, ZNF346, LBR, TPR
AURORA KINASE	3,21E-03	NPM1, CDC5L, PPP1R7, CBX5, BCAS2, CBX3, SUB1, CBX1, HNRNPK, SRSF3
PROTEIN PHOSPHATASE 1	3,81E-03	RPS6, CDC5L, SRSF10, PPP1R7, SF1, SF3B1, HSPA5, PPM1G, DNASE1L3, SEP15, RPSA
PROTEIN PHOSPHATASE 2	3,87E-03	RPS14, RPS3, LMNA, RBM17, ENSA, HNRNPU, BANF1, RPSA, ANP32E, ANP32A, FMR1, SET
ATAXIA TELANGIECTASIA MUTATED	3,87E-03	NUP153, BTF3, BCLAF1, CBX5, LMNB1, SMARCC2, KHSRP, PARP3, PPM1G, VRK1, PRPF19, HNRNPK
PROTEIN TYROSINE KINASE 6	4,39E-03	KHDRBS1, SFPQ, KHDRBS3, KHDRBS2
TUMOR PROTEIN P53	6,39E-03	NPM1, RPS14, EWSR1, EIF5A, RPS24, RPS19, HMGB3, HNRNPC, PSME3, RPS18, TAF9B, VRK1, PSMA5, DEK, TIAL1, RPL3, ZNF346, HNRNPK
PROTOONCOGENE / PROTEIN KINASE PIM	6,96E-03	EWSR1, RPS19, CBX5, CBX3, CBX1, API5

Table S2:

Proteins upregulated in the biotinylated dorsal surface fraction as compared to the ventral surface fraction:

Overrepresented pathways

Canonical pathway	P-value	List of observed genes
proteasome complex	1,22E-06	PSMD13, PSMC3, PSMD14, PSMD7, PSMC4, RPN1, PSMD12, PSMB2, PSMC6, PSMD6, PSMD11
Lissencephaly gene (LIS1) in neuronal migration and development	1,14E-04	CDK5, DYNC1H1, LRP8, CSNK2A1, VLDLR, LRPAP1, CDC42, PPP2R5D
spliceosomal assembly	3,93E-04	SNRPC, SNRPA1, SNRNP70, SNRPA
EPHB forward signaling	5,19E-04	TF, EFN2, RAP1B, EPHB4, EFN1, PTK2, CDC42, EFN3
PKA activation signaling (GPCR Dopamine D1like receptor signaling pathway)	7,90E-04	CDK5, CACNG4, CACNA1C, CACNB1, CACNA2D1, PPP2R5C, CACNB4, PPP2R5D, CACNG8
EphrinB-EPHB pathway	2,34E-03	EFNB2, EPHB4, EFN1
Posttranslational regulation of adherens junction stability and disassembly	2,59E-03	BDNF, CDH2, IGF1R, NTRK2, RAB7A, CDC42, CTNNA1, EGFR
Glypican 2 network	2,60E-03	GPC2, MDK
Reelin signaling pathway	2,91E-03	CDK5, GSK3B, LRP8, MAPT, VLDLR, LRPAP1
Netrin-mediated signaling events	4,14E-03	TRIO, UNC5A, UNC5B, PTK2, YES1, CDC42
N-cadherin signaling events	6,66E-03	CDH2, GRIA2, DAGLA, CDC42, CTNNA1, KIF5B
Nectin adhesion pathway	7,60E-03	RAP1B, PTK2, CDC42, PDGFRB, TLN1
agrin in postsynaptic differentiation	8,98E-03	AGRN, LAMC1, LAMB3, PTK2, CDC42, LAMA4, EGFR

Pathway	P-value	List of observed genes
GLUTAMATE RECEPTOR, IONOTROPIC, N METHYL D ASPARTATE	7,36E-09	GLUD1, DOCK3, CDK5, TACR1, BDNF, GRIK5, DLG3, RACK1, NTRK2, GRIA2, SLC1A3, EFN1, DLG1, PCDH10, EFN3, GRID1, NLGN1
TYROSINE PROTEIN KINASE FYN	2,07E-07	DOCK3, CDK5, LRP1, KHDRBS1, TRIO, PTPRF, LRP8, MAPT, NFAT5, RACK1, AGRN, MAP2, TYRO3, NTRK2, PAG1, SCN2A, GABRG2, UNC5B, VLDLR, PTK2, YES1, MCAM
CALCIUM/CALMODULIN DEPENDENT PROTEIN KINASE	8,97E-06	ACACA, KCND3, SLC6A1, BDNF, GRIK5, NRXN1, DLG3, ADRA2C, CACNA1C, MAP2, PHB2, GRIA2, PLCL2, SLC1A3, RAP1B, DAGLA, PHKA2, DLG1, KCNA4, KCNN4, KCND2, RAB10, NLGN1

METABOTROPIC GLUTAMATE RECEPTOR	2,07E-05	SLC6A1, GRIK5, GRIK3, MAP2, GNAL, GRIA2, SLC1A3, SLC1A6, GRM2, GRIA4, DAGLA, SLC1A2, GRM4, DLG1, ATXN2, GRM3, GRID2
POTASSIUM VOLTAGE GATED CHANNEL, KQT LIKE SUBFAMILY	2,04E-04	KCND3, CSNK2A1, KCNA1, SCN2A, LRPAP1, KCNA4, KCNN4, PRKCD
BRAIN DERIVED NEUROTROPHIC FACTOR (NEUROTROPHIN)	5,36E-04	DOCK3, SLC6A1, BDNF, EPHA7, RACK1, MAP2, MAGI1, NTRK2, NTRK3, SCN2A, GABRG2, ASIC2, LRIG1, SLC1A2, ADCYAP1R1
V YES 1 YAMAGUCHI SARCOMA VIRAL ONCOGENE HOMOLOG 1	7,11E-04	AGRN, TYRO3, IGF1R, PTK2, YES1, CDC42
PROTEIN PHOSPHATASE 2	9,91E-04	GSK3B, CSPG5, MAPT, PLPPR4, RACK1, CUL4B, CACNA1C, MAP2, RPSA, STRN3, PPP2R5C, UNC5B, PTPRO, LAMA4, NRXN2, PPP2R5D, STAG2, ANP32E, CDC7
NERVE GROWTH FACTOR	1,03E-03	BDNF, CDH13, MGLL, UNC5A, MAGI1, NTRK2, NTRK3, RAB7A, SMPD2, SLC8A1, ALCAM, LANCL1, HPSE, KIF5B, EFNB3
TRAFFICKING	1,09E-03	TACR1, TINAGL1, RAB12, LRP1, SLC6A1, CALCRL, GRIK5, CDH2, SGCD, ATRN, DLG3, CPSF6, SCFD1, RAB1A, LRP8, SYT7, SLC38A3, CACNA1C, MGRN1, LRSAM1, DOCK10, RAB7A, SACM1L, GRIA2, ASIC2, ARHGEF9, RAB1B, DAGLA, RALB, LRPAP1, SLC1A2, DLG1, STX12, LIN7C, EGFR, SNX27, KCND2, RAB10, ANP32E, KIF5B, PPM1L, KIF21A
NEUREGULIN	1,17E-03	CDK5, RTCB, ERBB4, CSPG5, AGRN, SLC1A6, EGFR, KCND2, CADM1
LEUCINE RICH REPEAT KINASE	1,58E-03	CDK5, MAPT, ANK1, RAB7A, PRDX3, CDC42, RPS15, RAB10
ANAPLASTIC LYMPHOMA KINASE	1,67E-03	SFPQ, IGF1R, PAG1, ATIC, MDK, EGFR, JAK3
EPH RECEPTOR	2,51E-03	PTPRF, EPHA7, RACK1, TYRO3, PAG1, AFDN, EFNB2, PTPRO, EPHB4, EFNB1, CACNB4, EFNB3
KV CHANNEL INTERACTING PROTEIN 3, CALSENILIN (DREAM)	2,65E-03	CDH2, GRK6, KCNIP4, KCND2
INSULIN RECEPTOR RELATED RECEPTOR	2,72E-03	IGF1R, NTRK2, MVD
PRESENILIN 1	3,15E-03	CDK5, GSK3B, CDH2, ERBB4, LRP8, MAPT, PAG1
LOW DENSITY LIPOPROTEIN RECEPTOR RELATED PROTEIN	3,34E-03	LRP1, LRP1B, CDH2, LRP8, AGRN, DVL2, PTK7, TF, VLDLR, GC, LRPAP1, PDGFRB, MDK, SPON1
VERY LOW DENSITY LIPOPROTEIN RECEPTOR	3,98E-03	LRP1, LRP8, VLDLR, LRPAP1, SPON1
PROTEIN KINASE C	4,26E-03	KCND3, SLC6A1, CSPG5, RACK1, SLC38A3, NOVA1, KCNA1, CHL1, RASGRP2, SCN2A, ELAVL1, GRIA2, SLC1A4, HNRNPK, ADGRL3, SLC8A1, UNC5B, SLC1A3, GRIA4, RALB, SLC8A3, TKT, ATP8B1, SLC1A2, CSPG4, CACNA1E, RPS11, ADCYAP1R1, PRKCD
FOCAL ADHESION KINASE 1	4,30E-03	TRIO, RTCB, SDCBP, CDH2, RACK1, RPSA, THSD7A, CSPG4, TNFR, PTK2, YES1, RGMA, HPSE, SPON1, TLN1, MCAM, LIN7C, TENM4

TYROSINE PROTEIN KINASE SRC	5,20E-03	KCND3, KHDRBS1, TRIO, SDCBP, RACK1, PAG1, PLXNB1, AFDN, FERMT2, HNRNPK, SMPD3, RAP1B, PTPRO, PTK2, YES1, CACNB4, ATP5J, PDGFRB, HPSE, SPON1, EGFR, PRKCD
ADRENERGIC RECEPTOR	5,64E-03	GRK6, ADRA2C, ADCY1, CACNA1C, MAP2, SLC24A3, GRM4, PDGFRB, RAP1GAP, KCND2
PLANAR CELL POLARITY	5,74E-03	EPHA7, ASTN1, SESTD1, DVL2, PTK7, GPC4, DCHS1, DLG1
PROTEIN TYROSINE KINASE 6	5,92E-03	KHDRBS1, SFPQ, PTK2, YES1, EGFR
REELIN	6,50E-03	CDK5, LRP1, CDH2, LRP8, VLDLR, LRPAP1, SPON1
REDOX	6,82E-03	GLUD1, ACOX1, HCFC1, PTPRS, TF, POR, SMPD3, CAT, GSPT1, LANCL1, APEX1, PRDX3, DAO, PDGFRB, KCNA4, ATXN2, SORD
ENDOCYTIC	7,25E-03	TACR1, RAB12, LRP1, EPS15L1, GRIK5, LRP8, SYT7, ATP6V1H, MAP1LC3A, NTRK2, SCN2A, DVL2, RAB7A, TF, PDCD5, GC, LRPAP1, ALCAM, APOB, FGFR2, CDC42, VTA1, EGFR, SNX27
SEMAPHORIN	7,76E-03	CDK5, FARP1, SEMA4F, PLXNB1, PTK7, GRIA2, NRP2, PLXNA4, PLXNA2

Table S3:

Proteins upregulated in the surface fraction of young brains: Overrepresented pathways

Canonical pathway	P-value	List of observed genes
proteasome complex	1,22E-06	PSMD13, PSMC3, PSMD14, PSMD7, PSMC4, RPN1, PSMD12, PSMB2, PSMC6, PSMD6, PSMD11
spliceosomal assembly	1,63E-05	SNRPC, U2AF2, SNRPA1, SNRNP70, SNRPA
EphrinB-EPHB pathway	9,13E-05	EPHB1, EFN2, EPHB4, EFN1
Lissencephaly gene (LIS1) in neuronal migration and development	1,14E-04	CDK5, DYNC1H1, LRP8, CSNK2A1, VLDLR, LRPAP1, CDC42, PPP2R5D
PKA activation signaling (GPCR Dopamine D1like receptor signaling pathway)	1,62E-04	CDK5, CACNG4, PPP2R5E, CACNA1C, CACNB1, CACNA2D1, PPP2R5C, CACNB4, PPP2R5D, CACNG8
deregulation of cdk5 in alzheimers disease	3,92E-04	CDK5, GSK3B, MAPT, PPP2R5D
EPHB forward signaling	5,18E-04	EPHB1, EFN2, RAP1B, EPHB4, EFN1, PTK2, CDC42, EFN3

Posttranslational regulation of adherens junction stability and disassembly	5,77E-04	BDNF, CDH2, CTNNB1, IGF1R, NTRK2, RAB7A, CDC42, CTNNA1, EGFR
N-cadherin signaling events	1,34E-03	CDH2, CTNNB1, GRIA2, DAGLA, CDC42, CTNNA1, KIF5B
Reelin signaling pathway	2,90E-03	CDK5, GSK3B, LRP8, MAPT, VLDLR, LRPAP1
Filopodium formation (Integrin signaling pathway)	3,53E-03	DOCK3, SMC3, AGRN, TNC, DOCK10, GPC1, LAMB3, GPC4, COL15A1, RAP1B, NCAN, PTK2, CDC42, TLN1
Netrin-mediated signaling events	4,13E-03	TRIO, UNC5A, UNC5B, PTK2, YES1, CDC42
Syndecan-4-mediated signaling events	4,88E-03	SDCBP, PLG, TNC, PTK2, MDK, PRKCD
agrin in postsynaptic differentiation	8,96E-03	AGRN, LAMC1, LAMB3, PTK2, CDC42, LAMA4, EGFR

Pathway	P-value	List of observed genes
GLUTAMATE RECEPTOR, IONOTROPIC, N METHYL D ASPARTATE	1,16E-09	GLUD1, DOCK3, CDK5, TACR1, BDNF, GRIK5, DLG3, EPHB1, GNB2L1, AGRN, NTRK2, GRIA2, SLC1A3, EFNB1, DLG1, EFNB3, GRID1, NLGN1
TYROSINE PROTEIN KINASE FYN	2,02E-07	DOCK3, CDK5, TRIO, BDNF, MAG, LRP8, MAPT, FLOT1, NFAT5, GNB2L1, PTPRC, AGRN, MAP2, TYRO3, NTRK2, PAG1, SCN2A, GABRG2, UNC5B, PTK2, YES1, CTNNA1
METABOTROPIC GLUTAMATE RECEPTOR	9,84E-07	SLC6A1, GRIK5, GRIK3, MAP2, GRM8, GNAL, GRIA2, SLC1A3, GRM2, GRIA4, DAGLA, SLC1A2, GRM4, DLG1, ATXN2, GRM6, GRM3, GRID2
SEMAPHORIN	1,20E-05	CDK5, GSK3B, MAG, FLOT1, NRCAM, SEMA4F, PLXNB1, PTK7, GRIA2, NRP2, PLXNA4, PLXNA2, PTK2, PLXND1
CALCIUM/CALMODULIN DEPENDENT PROTEIN KINASE	1,37E-05	ACACA, SLC6A1, BDNF, GRIK5, NRXN1, DLG3, ADRA2C, CACNA1C, MAP2, PHB2, LRRTM1, SLC1A3, RAP1B, DAGLA, PHKA2, DLG1, KCNA4, KCNN4, KCND2, RAB10, OLFM1, NLGN1
ANAPLASTIC LYMPHOMA KINASE	5,14E-05	SFPQ, FLOT1, IGF1R, PAG1, RPS6, ATIC, MDK, EGFR, JAK3
INSULIN RECEPTOR RELATED RECEPTOR	1,51E-04	IGF1R, NTRK2, INSRR, MVD
NERVE GROWTH FACTOR RECEPTOR	2,47E-04	BDNF, CDH13, MGLL, MAG, UNC5A, SLC8A2, MAGI1, NTRK2, RAB7A, SMPD2, SLC8A1, ALCAM, LANCL1, HPSE, OLFM1, EFNB3
PROTEIN PHOSPHATASE 2	3,03E-04	CDK5, GSK3B, CSPG5, PPP2R5E, MAPT, GNB2L1, CUL4B, CACNA1C, MAP2, RPSA, STRN3, U2AF2, PPP2R5C, UNC5B, ACSL1, LAMA4, NRXN2, PPP2R5D, STAG2, ANP32E, CDC7
LOW DENSITY LIPOPROTEIN RECEPTOR RELATED PROTEIN	4,15E-04	LRP1, GSK3B, LRP1B, MAG, PPP2R5E, LRP8, RAB8B, AGRN, CTNNB1, DVL2, PTK7, VLDLR, GC, LRPAP1, MDK, SPON1
POTASSIUM VOLTAGE GATED CHANNEL, KQT LIKE SUBFAMILY	4,38E-04	CSNK2A1, SCN2A, KCNA2, LRPAP1, KCNA4, KCNN4, PRKCD

NEUREGULIN	4,80E-04	CDK5, RTCB, ERBB4, CSPG5, AGRN, GABRB2, SLC1A6, EGFR, KCND2, CADM1
EPH RECEPTOR	4,84E-04	EPHA7, EPHB1, NRCAM, GNB2L1, TYRO3, PAG1, MLLT4, EFN2, PTPRO, EPHB4, EFN1, CACNB4, EFN3
CADHERIN 2, TYPE 1, N CADHERIN (NEURONAL)	5,83E-04	CDH2, ROBO2, CTNNB1, NOTCH3, MLLT4, EFN1, FGFR2, CTNNA1, CDH11, NLGN1
CADHERIN 13, H CADHERIN (HEART)	6,03E-04	GSK3B, CDH13, CDC42, EGFR, SOGA1
BRAIN DERIVED NEUROTROPHIC FACTOR (NEUROTROPHIN)	6,48E-04	DOCK3, SLC6A1, BDNF, EPHA7, MAG, NRCAM, GNB2L1, MAP2, MAG1, NTRK2, SCN2A, GABRG2, ASIC2, SMPD2
FOCAL ADHESION KINASE 1	7,54E-04	TRIO, RTCB, SDCBP, EPHB1, GNB2L1, TNC, RPSA, NRP2, THSD7A, CSPG4, PTK2, RGMA, CDC42, HPSE, SPON1, TLN1, LIN7C, POSTN, TENM4
REELIN	8,64E-04	CDK5, LRP1, CDH2, LRP8, VLDLR, LRPAP1, SPON1, KCNJ3
INTEGRIN LINKED KINASE	1,66E-03	GSK3B, CDH13, MAPT, ANK1, CTNNB1, FERMT2, ELMO2, PTK2, CDC42, TLN1
PTK2B PROTEIN TYROSINE KINASE 2 BETA	1,84E-03	LRP1, LRP1B, DLG3, SLC8A2, PLXNB1, KCNA2, CSPG4, PTK2, EGFR, ADCYAP1R1, PRKCD
PRESENILIN 1	1,89E-03	CDK5, GSK3B, ERBB4, LRP8, MAPT, CTNNB1, PAG1
VERY LOW DENSITY LIPOPROTEIN RECEPTOR	2,81E-03	LRP1, LRP8, VLDLR, LRPAP1, SPON1
V YES 1 YAMAGUCHI SARCOMA VIRAL ONCOGENE HOMOLOG 1	4,37E-03	AGRN, TYRO3, IGF1R, YES1, CDC42
PHOSPHOLIPASE D	4,73E-03	CDK5, MBOAT2, DAGLA, ATP8B1, JAK3, ADCYAP1R1, PRKCD
INTEGRIN	4,76E-03	ANK1, PLG, PTPRC, AGRN, CHL1, TNC, DOCK10, FERMT2, MRC2, CSPG4, TNF, PTK2, CDC42, HPSE, TLN1, POSTN
CYCLIN G1	6,15E-03	CDK5, PCNA, NOTCH3, PPP2R5C
MACROPHAGE STIMULATING 1 RECEPTOR (C MET RELATED TYROSINE KINASE) (RON)	6,15E-03	PCNA, CTNNB1, TYRO3, IGF1R
TYROSINE PROTEIN KINASE SRC	6,46E-03	TRIO, SDCBP, EPHB1, GNB2L1, PTPRC, PAG1, TNC, PLXNB1, MLLT4, FERMT2, SMPD3, RAP1B, PTPRO, PTK2, YES1, CACNB4, ATP5J, CDC42, HPSE, SPON1, EGFR, PRKCD
CASEIN KINASE 1	6,95E-03	DDX3X, GSK3B, MAPT, NFAT5, CSNK2A1, CTNNB1, DVL2, RPS6, CDC7, PPM1L
PAXILLIN	7,37E-03	RTCB, EPHB1, GNB2L1, PTPRO, ATP8B1, PTK2, CDC42, TLN1, CTNNA1, ADCYAP1R1
ADRENERGIC RECEPTOR	7,37E-03	TACR1, GRK6, ADRA2C, ADCY1, CACNA1C, MAP2, GRM4, RAP1GAP, KCNJ3, KCND2

TRAFFICKING	8,17E-03	TACR1, TINAGL1, RAB12, LRP1, SLC6A1, BDNF, CALCRL, SGCD, ATRN, DLG3, SCFD1, LRP8, FLOT1, RAB8B, MGRN1, RAB6A, LRSAM1, DOCK10, RAB7A, SACM1L, GRIA2, KCNA2, ASIC2, RAB1B, RALB, LRPAP1, SLC1A2, RAB35, DLG1, LIN7C, EGFR, ADCYAP1R1, SNX27, KCND2, ANP32E, KIF5B, PPM1L, KIF21A
ENDOCYTIC	8,70E-03	TACR1, RAB12, LRP1, EPS15L1, LRP8, FLOT1, RAB6A, ATP6V1H, SCN2A, DVL2, RAB7A, PDCD5, GC, LRPAP1, ALCAM, FGFR2, CDC42, RAB35, LASP1, VTA1, EGFR, SNX27, RAB10

Biological processes:

cell cycle G1/S phase transition	2,03E-07	PSMD1, UBA52, DDX3X, PSMD13, PSMC3, PSMD14, PSMD2, CUL4B, PCNA, PHF8, PHB2, PSMD7, PSMC4, PRKDC, CUL1, RPS6, PPP2R5C, PSMD12, GSPT1, PSMB2, EGFR, PSMC6, PSMD6, CDC7, PSMD11
----------------------------------	----------	--

Table S4:

Proteins upregulated in the surface fraction of old brains: overrepresented pathways

Canonical pathway	P-value	List of observed genes
gamma-aminobutyric acid receptor life cycle pathway	1,35E-04	UBE3A, NSF, CLTA, CLTC, UBA1, GPHN
CXCR3-mediated signaling events	2,97E-04	GNAO1, ITGB2, MAP2K1, GNAI1, GNAI2, MAPK1, MAP2K6, ARRB1
role of erbb2 in signal transduction and oncology	1,83E-03	LRPPRC, MAP2K1, CARM1, MAPK1, STAT3, GRB2
S1P1 pathway	2,16E-03	GNAO1, ITGAV, GNAI1, GNAI2, MAPK1
NGF signaling pathway (NGF signaling pathway)	2,72E-03	SHC3, MAP2K1, BRAF, MAPK1, GRB2
S1P4 pathway	3,63E-03	GNAO1, GNAI1, GNAI2, MAPK1
PDGFR-beta signaling pathway	4,12E-03	PPP2R2B, ITGAV, MAP2K1, BRK1, YWHAQ, YWHAE, BRAF, PTEN, CTTN, MAPK1, STAT3, GRB2, YWHAB
LKB1 signaling events	4,64E-03	PRKACA, MAP2, YWHAQ, YWHAE, CAB39, BRSK1, YWHAB

AKT(PKB) activation signaling (Insulin receptor signaling)	4,73E-03	PPP2R2B, SHC3, MAP2K1, YWHAQ, YWHAE, BRAF, PTEN, MAPK1, GRB2, YWHAB
S1P5 pathway	5,23E-03	GNAO1, GNAI1, GNAI2
Class IB PI3K non-lipid kinase events	6,67E-03	MAP2K1, MAPK1
AKT(PKB) activation signaling (Insulin receptor signaling (Mammal))	6,71E-03	PPP2R2B, SHC3, MAP2K1, YWHAQ, YWHAE, BRAF, PTEN, MAPK1, GRB2, YWHAB
G alpha s GDP-GTP exchange signaling (GPCR Adenosine A2A receptor signaling pathway)	6,86E-03	PRKACA, PRKAR2A, MAP2K1, BRAF, GNB5, MAPK1
Hedgehog signaling events mediated by Gli proteins	7,58E-03	PRKACA, XPO1, GNAO1, MAP2K1, GNAI1, GNAI2, RBBP4
Nongenotropic Androgen signaling	8,53E-03	GNAO1, MAP2K1, GNAI1, GNAI2, MAPK1
EGF receptor proximal signaling	8,53E-03	GNAI1, GSN, MAPK1, STAT3, GRB2
S1P3 pathway	9,98E-03	GNAO1, ITGAV, GNAI1, GNAI2, MAPK1

REDOX	5,42E-07	TIAM1, PRDX5, AIFM1, MCCC2, GLRX3, TXNRD3, GPD1L, LANCL2, FDXR, ERP44, ATP5A1, TARDBP, CTH, PRDX6, ACADS, GSTZ1, TRPM2, FLAD1, GPX4, PRDX1, NNT, NAMPT, PRDX2, IMMT, SOD2, GOT1, CYB5R1, DSCR3
TRAFFICKING	1,36E-06	RAB14, HSPA8, TUBA1B, STXBP3, DNPEP, TNPO3, STXBP1, SNAP25, STAM2, VWF, RAB27B, NAE1, XPO1, OSBP, NEFL, PICALM, MPZ, ERP44, TSG101, SYN1, NDRG4, S100B, APPL1, ATP5A1, SLC6A9, MINK1, RIN1, DYNC1LI1, RAP1GDS1, MUT, NEDD4L, NSF, GIT1, FLOT2, SHANK2, DLG4, ANXA2, PPIA, CHM, ASNA1, ST13, RAB35, BCR, PITPNA, GJA1, TPM3, TOLLIP, KPNA3, DCTN2, RAB3GAP1, PANX1, SNAP91, SNX13, TXNL1, GPHN, GAD2, ARRB1
CALCIUM/CALMODULIN DEPENDENT PROTEIN KINASE	3,95E-04	TIAM1, DNM1L, OGT, FTO, NCAM1, PEA15, SNAP25, PRKACA, SYP, NEFL, MAP2, SYN1, PPM1F, GIT1, DLG4, NPTX2, CAMKK1, PPM1E, BRSK1, GLO1, GPHN
ENDOCYTIC	5,51E-04	RAB14, RECK, HSPA8, INPP5F, STAM2, HTATIP2, SYP, PICALM, NCKIPSD, TSG101, APPL1, RUVBL2, HEPH, RIN1, SNX2, NSF, HOOK1, GIT1, ANXA2, GGA3, CHM, SRGAP3, RAB35, CLTC, TOLLIP, DCTN2, PANX1, SNAP91, SNX13, ARRB1
AMYLOID BETA (A4) PRECURSOR PROTEIN	6,81E-04	DNM1L, UCHL1, NAE1, SYP, ANKS1B, PICALM, HSD17B10, S100B, TARDBP, VDAC1, GFAP, GNAI2, APLP2, CLU
STRESS	7,98E-04	COMT, PRDX5, OGT, LOXL4, LMNB1, BLVRA, PSAP, TARDBP, ATG7, PRDX6, TRPM2, SDHA, GPX4, VDAC2, PRDX1, ATG3, LONP1, ASPG, AK1, CLTC, PRDX2, SOD2, TPM3, GLO1, GCLM, CLPP

DEATH RECEPTOR	9,34E-04	EIF3F, DNM1L, PRDX5, MTCH2, AIFM1, AGL, PEA15, LMNB1, ALDH1L1, RGS6, NAE1, HTATIP2, HYOU1, LRPPRC, PSAP, HK1, HSPA5, LARP6, PRPS2, CASP10, VDAC1, ATG7, ESD, ITGB4, CSE1L, CALB2, CYC1, TRPM2, SDHA, DAB2IP, GPX4, VDAC2, HINT1, EEF1A1, PRDX1, GSN, CLU, NPTX1, EIF2A, PRDX2, SOD2, GLO1, CLPP, HSPD1, TXNL1
PROTEIN PHOSPHATASE 2	1,00E-03	PPP2R2B, DNM1L, EIF2S2, SNAP25, LCMT1, GLRX3, NEFL, NDRG2, PDE1A, MAP2, PPP2R2A, PPME1, MINK1, NEFH, PPM1B, EIF2B1, PSAT1, CCDC22, PPP6C, GJA1, RAB3GAP1, GPHN
P21(CDKN1A) ACTIVATED KINASE	1,07E-03	SYNJ1, TIAM1, ITGB5, NCAM1, RUFY3, DYNLL2, SYN1, MAP2K1, PGAM1, GIT1, CTTN, FOLH1, GJA1, PGM1
NEUROTROPHIC TYROSINE KINASE RECEPTOR	1,34E-03	TIAM1, TUBA1B, NCAM1, ACHE, SHC3, SYN1, APPL1, NEDD4L, CNDP2, DLG4, NPTX2, GGA3, GAD2
PROTEIN KINASE C	3,12E-03	TIAM1, TUBA1B, STXBP3, STXBP1, PEA15, SNAP25, VWF, GLRX3, LMNB1, GPD1L, OSBP, NEFL, MPZ, DBH, S100B, LPCAT2, ACO1, ELAVL1, SLC6A9, CAPZB, H3F3B, PCYT2, NSF, PEBP1, HINT1, ANXA2, ELAVL4, SUSDS5, NDUFS2, GPM6A, PPP1R12A, RPL6, FSCN1, PITPNA, GJA1
GLYCOGEN SYNTHASE KINASE	4,05E-03	DNM1L, LCMT1, XPO1, NDRG2, NEFM, NEB, DPYSL3, MAP2, VDAC1, ECHS1, KLC2, GDI2, NEFH, PTEN, PSAT1, SIRT2, AK1, NPTX1, ARNTL, CLASP2, GPHN
REELIN	9,18E-03	COMT, PAFAH1B1, PAFAH1B2, CRMP1, CALB2, NOVA2, DAB2IP
METABOTROPIC GLUTAMATE RECEPTOR	9,25E-03	MAP2, SYN1, KLC2, GFAP, SHANK3, NSF, DLG4, NPTX2, EEF1A1, PVALB, NPTX1, GPHN
SPROUTY HOMOLOG (DROSOPHILA)	9,58E-03	RECK, ENAH, BRAF, PTEN, NF1, MAPK1, GPHN, GRB2

Table S5: summary of all IGF2b overexpression experiments

	Experiment 1+2 (+4d)		Experiment 3 (+5d)		Experiment 4 (+2d)		Experiment 5 (+5d)		Experiment 6 (+3d)		Experiment 7 (+4d)	
young-CTR	0,0%	n=16	18,8%	n=16		n=0	36,4%	n=11	40,0%	n=5	14,3%	n=21
young-IGF	25,0%	n=16	28,6%	n=14	31,8%	n=22	75,0%	n=12	25,0%	n=8	54,8%	n=42
old-CTR	0,0%	n=10	7,1%	n=14		n=0	27,3%	n=11	0,0%	n=6	26,1%	n=23
old-IGF	50,0%	n=18	27,3%	n=11	33,3%	n=3	0,0%	n=8	0,0%	n=5	42,9%	n=28